

# Heating of Galactic Disks by Infalling Satellites

A. J. Benson<sup>1</sup>, C. G. Lacey<sup>2</sup>, C. S. Frenk<sup>2</sup>, C. M. Baugh<sup>2</sup> & S. Cole<sup>2</sup>

1. California Institute of Technology, MC 105-24, Pasadena, CA 91125, U.S.A. (e-mail: abenson@astro.caltech.edu)

2. Physics Department, University of Durham, Durham, DH1 3LE, England

7 February 2020

## ABSTRACT

We develop an analytic model to calculate the rate at which galaxy disks are heated by dark matter substructures orbiting in their halos. We calibrate this model against new N-body simulations and demonstrate that it is able to reproduce the N-body heating rates to within a factor of 2 in the majority of cases. Applying these calculations within a model for the growth of disk galaxies in a  $\Lambda$ -dominated cold dark matter universe, we predict the distribution of disk scale heights for galaxies of different luminosities. For  $L_*$  spiral galaxies, we predict that the median disk thickness is only 5% of the radial scalelength if substructure is the only source of disk heating. However, the median disk thickness increases to nearly 20% of the radial scalelength when heating due to gravitational scattering of stars by molecular clouds is also included. This latter value is close to the disk thickness estimated observationally for the Milky Way galaxy. The distribution of disk thicknesses predicted by the model is also consistent with a recent observational determination of the thickness distribution for sub- $L_*$  disk galaxies by Bizyaev & Mitronova (2002). Thus, the observed thicknesses of the stellar disks of spiral galaxies seem to be entirely consistent with the abundance of substructure in dark matter halos predicted by the standard  $\Lambda$ -dominated cold dark matter model. Universes with  $\Omega_0 = 1$  predict similar scale-heights for our current best model of galaxy formation in this cosmology, a consequence of the fact that similar amounts of substructure are accreted by halos in  $\Omega_0 = 1$  and  $\Omega_0 = 0.3$ ,  $\Lambda_0 = 0.7$  cosmologies during the lifetimes of their respective disks.

## 1 INTRODUCTION

A generic prediction of hierarchical models of structure formation, such as the cold dark matter (CDM) model, is that the dark matter halos of galaxies and clusters should contain large amounts of substructure, in the form of small, gravitationally-bound subhalos orbiting within the larger potential. This substructure arises because large halos are built up by merging of smaller halos, and the subhalos are the tidally-stripped remnants of the small halos which merged into the larger system. Recently, it has been claimed that the CDM model predicts an order of magnitude too many subhalos around the Milky Way galaxy, compared to what one infers from the number of satellite galaxies (Moore 2001; Klypin et al. 1999). Several authors have now pointed out that this apparent discrepancy is readily explained if some process (such as the heating of the intergalactic medium (IGM) during reionization) is efficient at suppressing the formation of galaxies in most of these subhalos (Bullock, Kravtsov & Weinberg 2000; Somerville 2002; Benson et al. 2002b). A consequence of this picture is that galaxy halos should be filled with many small subhalos containing negligible amounts of luminous material. A strong test of this scenario is therefore to search for gravita-

tional signatures of these subhalos, bypassing the problems of relating subhalos to the visible material in satellite galaxies.

Perhaps the most direct method of searching for substructure in dark matter halos is to look for gravitational microlensing signatures. This particular constraint is now reasonably well studied theoretically (Metcalf & Madau 2001; Chiba 2002; Dalal & Kochanek 2002a; Dalal & Kochanek 2002b). Although the interpretation of the current datasets leaves some uncertainty, all studies so far find the observed microlensing rates to be consistent with the abundance of substructure predicted by CDM.

An alternative constraint on the amount of substructure in halos can be obtained by considering the thicknesses of the stellar disks of galaxies. Subhalos on orbits which pass through a galactic disk will gravitationally perturb the disk and deposit energy into it, gradually heating it and increasing its scale-height. Since other mechanisms also heat the stellar disks of galaxies (but with uncertain efficiency), the observed thicknesses of galactic disks set an upper limit on the abundance of such substructure. The heating of galactic disks by infalling satellites was first developed as a constraint on models of structure formation by Tóth & Ostriker (1992; hereafter TO). They calculated this effect semi-analytically,

and concluded that the thinness of the Milky Way's disk is inconsistent with the hierarchical build-up of galaxies in a high density ( $\Omega = 1$ ) CDM universe. Subsequent numerical simulations of single mergers of satellites with larger disk galaxies (e.g. Huang & Carlberg 1997; Velázquez & White 1999) indicated that TO's analytical estimates of the heating rate were somewhat too high, weakening their constraint on structure formation models. More recently, Font et al. (2001) have numerically simulated the heating of disks by the ensemble of subhalos predicted to exist within dark halos in the CDM model. Their simulations of Milky Way-like galaxies only set an upper limit to the rate of disk heating by satellites, because of numerical effects, but they conclude that this is less than the total disk heating rate that is inferred observationally for the solar neighbourhood. They argue that the heating rates are low because there are few of the most massive satellites (which cause the most heating) and because few satellites penetrate the inner regions of the disk. Their conclusions are however limited by the fact that they simulated only two realizations of the halo substructure.

In this paper we develop a new semi-analytical model of disk heating by halo substructure. This model builds on earlier semi-analytical modelling of galaxy formation within the framework of CDM (Cole et al. 2000), and on recently-developed analytical models for the evolution of satellites within dark matter halos (Taylor & Babul 2001; Benson et al. 2002a; Taffoni et al. 2003; Taylor & Babul 2003). The rate at which satellite halos of different masses join the main halo through merging is predicted by the galaxy formation model. The satellite model then predicts how the masses, radii and orbits of subhalos evolve due to dynamical friction and tidal stripping by the halo, disk and bulge of the host galaxy. In this paper, we add a calculation of how much of the orbital energy of the satellites that is lost by dynamical friction goes into increasing the thickness and vertical motions of the galactic disk. We test and calibrate our analytical model of satellite evolution against a set of high-resolution N-body simulations of single satellites merging with disk galaxies. We find (as has also been shown by Taylor & Babul 2001 and Taffoni et al. 2003) that such an analytical model is able to reproduce well the behaviour seen in N-body simulations. We measure the disk heating in the same simulations, and find that it is quite well reproduced by our analytical model. We then go on to apply this model of heating by satellites within the framework of our semi-analytical model of galaxy formation, in order to predict the distribution of scaleheights for disk galaxies of different luminosities.

Both the N-body and semi-analytical approaches have advantages and disadvantages as applied to this problem. N-body simulations have the advantage of fully accounting for the non-linear interaction of substructure and disk (e.g. accounting for the excitation of global modes such as warps and bars in the disk). However, they are limited by resolution and artificial numerical heating, and typically have been able to consider only a small number of realizations (e.g. two realizations, in the case of the best cosmological simulations of disk heating to date, by Font et al. ). The semi-analytical

approach has the advantage of not being limited by resolution or artificial heating, and of allowing the calculation of a large number of realizations. Since heating by substructure is a highly stochastic process, it is important to account for the galaxy-to-galaxy variation in the heating rate by calculating a large number of realizations. At present, only the semi-analytical approach allows this.

The remainder of this paper is arranged as follows. In §2 we describe our analytical model for disk heating by subhalos and for the evolution of the disk scale-height. In §3 we calibrate and test our analytical model against numerical simulations of single satellite-disk mergers. In §4 we present our predictions for the distribution of scaleheights of disk galaxies in the CDM model, and compare with observational data for the Milky Way and for other galaxies. Finally, in §5 we present our conclusions. Appendices detail derivations of various formulae related to dynamical friction and disk energies.

## 2 MODEL

### 2.1 Evolution of Satellites and their Orbits

We calculate the evolution of the masses, radii and orbits of satellites using a development of the model presented in Benson et al. (2002a; hereafter Paper I). That work in turn was based on the satellite evolution model of Taylor & Babul (2001). We summarize here the main features of our model: The growth of the main halo is described by a merger history tree which is calculated by a Monte Carlo method (Cole et al. 2000). When smaller halos (in general containing one or more visible galaxies) merge with the main halo, they become satellite halos. The satellite halos are given initial orbits which start close to the virial radius but have a range of eccentricities. The satellite orbits are followed in the potential of the host system, and evolve due to dynamical friction against the dark halo, disk and bulge of the main galaxy. At the same time, the satellites lose mass by tidal stripping, both "static" tidal limitation and tidal shocking. As a satellite is tidally stripped, its radius and internal structure also change.

We have made a few improvements to our satellite orbit model from that presented in Paper I. These are described in Appendix A.

### 2.2 Disk Heating

#### 2.2.1 Rate of Heating

We now wish to calculate the rate at which a satellite halo heats the disk of the galaxy in its host halo. The satellite experiences dynamical friction against the disk, and the energy lost from the orbital motion of the satellite by this mechanism goes into increasing the energy of the disk. Working in the frame in which the centre of mass of the central galaxy and its halo are at rest, the satellite injects energy into the disk at a rate

$$P = \mathbf{F}_{\text{df},\text{disk}} \cdot \mathbf{v}_{\text{sat}}, \quad (1)$$

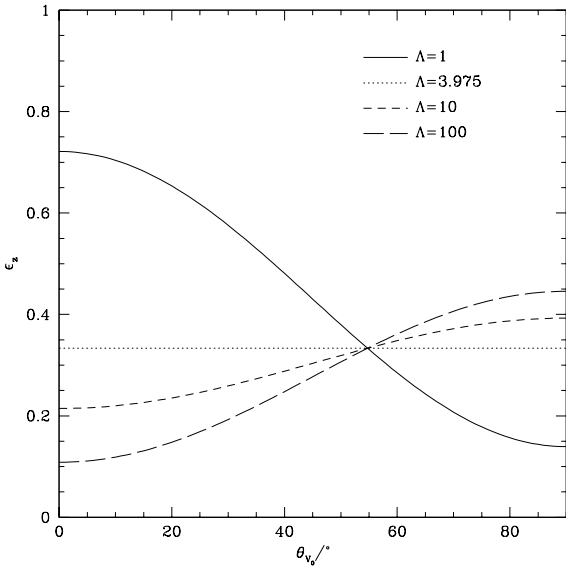


**Figure 1.** The efficiency of energy transfer to vertical motions in the disk as a function of the angle between the disk-satellite relative velocity and the  $z$ -axis,  $\theta_{V_0}$ . Results are plotted for several values of  $\Lambda$  as indicated in the figure.

where  $\mathbf{F}_{\text{df},\text{disk}}$  is the dynamical friction force exerted by the disk and  $\mathbf{v}_{\text{sat}}$  is the velocity of satellite. This energy is initially injected in the form of kinetic energy, but is then mixed between kinetic and potential energies by the motions of the stars. We are interested in the increase in the vertical energy of the disk, which is given by

$$\dot{E}_z = \epsilon_z \mathbf{F}_{\text{df},\text{disk}} \cdot \mathbf{v}_{\text{sat}}, \quad (2)$$

We derive an expression for the efficiency factor  $\epsilon_z \leq 1$  in Appendix B3 by considering the increases in the vertical and horizontal components of the velocity dispersion of the stars responsible for dynamical friction during scattering events. This expression (B29) depends only on the Coulomb logarithm,  $\ln \Lambda$ , and the angle  $\theta_{V_0}$  between the disk-satellite relative velocity and the  $z$ -axis. We then simply integrate  $\dot{E}_z$  along the satellite orbit to determine the net increase in the disk's vertical energy.

Figure 1 shows  $\epsilon_z$  for a few representative values of  $\Lambda$ . Note that  $\epsilon_z = \frac{1}{3}$  when  $\cos \theta_{V_0} = \frac{1}{\sqrt{3}}$ , independent of  $\Lambda$ . For small  $\Lambda$  the efficiency is greatest when  $\theta_{V_0} = 0^\circ$  (approaching unity as  $\Lambda$  approaches zero) and smallest for  $\theta_{V_0} = 90^\circ$  (approaching zero as  $\Lambda$  approaches zero). For large  $\Lambda$  the trend is reversed, with  $\epsilon_z$  being smallest at  $\theta_{V_0} = 0^\circ$  (approaching zero as  $\Lambda$  approaches infinity) and largest for  $\theta_{V_0} = 90^\circ$  (approaching  $\frac{1}{2}$  as  $\Lambda$  approaches infinity). The transition between these two regimes occurs for  $\Lambda \approx 3.975$ , for which  $\epsilon_z$  is independent of  $\theta_{V_0}$ .

We can understand the behaviour of  $\epsilon_z$  in simple terms. For example, for  $\theta_{V_0} = 0$  the efficiency drops to zero as  $\Lambda$  becomes large. In this case, vertical motions in the disk are parallel to the relative velocity vector of the satellite and the disk stars. Consequently, only the  $\Delta V_{m\parallel}$  term (see

eqn. B15) contributes to increasing the energy in these vertical motions. For large impact parameters,  $b$ , the increase in velocities (and hence energies) perpendicular to the satellite motion dominates over that parallel to the motion, since  $\Delta V_{m\parallel} \propto b^{-2}$  while  $\Delta V_{m\perp} \propto b^{-1}$  (see eqn. B16)\*. As  $\Lambda$ , and hence the maximum impact parameter, increases energy transfer from the satellite becomes dominated by large  $b$  scatterings. Consequently, the efficiency of transfer to vertical motions in the disk drops to zero as  $\Lambda$  becomes large.

The reversal of the trend of  $\epsilon_z$  with  $\theta_{V_0}$  at  $\Lambda \approx 3.975$  is also simple to understand. For larger  $\Lambda$  energy transfer is always predominantly into motions perpendicular to the motion of the satellite (as discussed above). As such, the efficiency of energy transfer to motions in the vertical direction are greatest when the satellite moves perpendicular to that direction ( $\theta_{V_0} = 90^\circ$ ). For smaller  $\Lambda$ , energy transfer occurs mostly into the parallel direction, and so  $\epsilon_z$  is maximized for  $\theta_{V_0} = 0^\circ$ . For  $\Lambda \approx 3.975$  energy transfer into perpendicular and parallel directions is equal and so  $\epsilon_z$  is constant. When  $\cos \theta_{V_0} = \frac{1}{\sqrt{3}}$  the energy transferred to vertical motions is always one third of the increase in energies parallel to the satellite velocity plus one third of the increases in energies in the two directions perpendicular to the satellite velocity. As such, this energy is always exactly one third of the total energy transferred from the satellite and hence  $\epsilon_z = \frac{1}{3}$  independent of  $\Lambda$ .

### 2.2.2 Disk Scale Height and Vertical Energy

Having calculated the energy deposited into vertical motions of disk stars, we now wish to calculate the resulting scale height of the disk. We work throughout in the *thin disk approximation*, meaning that the vertical extent of the disk is assumed to be small compared to its radial extent, and also that the non-circular velocities are small compared to the circular velocity. In this approximation, the disk can be treated as being locally plane-parallel, with the consequence that the vertical motions separate from the motions in the plane, and there is a well-defined vertical energy which (in the absence of perturbations by satellites or other objects) is conserved both for individual stars and for the disk as a whole. The vertical energy given to a star by an encounter with a satellite is initially in the form of vertical kinetic energy, but the orbital motion of the star subsequently mixes this between vertical kinetic and potential energies, while

\* This difference in the scaling of  $\Delta V_{m\parallel}$  versus  $\Delta V_{m\perp}$  is also easy to understand. The dependence of  $\Delta V_{m\perp}$  for large  $b$  is easily calculated by integrating the perpendicular component of the gravitational force due to the satellite along the unperturbed orbit of the particle being scattered (which is simply uniform motion along a straight line, with closest approach  $b$  to the satellite). Integrating the parallel component of the gravitational force along this same orbit yields zero net change in the parallel component of velocity (as is obvious from the symmetry of the problem). To find the change in the parallel velocity we must therefore integrate the parallel component of the gravitational force along the *perturbed* orbit. As such, the change in velocity parallel to the direction of motion is seen to be a second order effect and consequently scales as  $b^{-2}$  instead of  $b^{-1}$ .

**Table 1.** Details of the galaxy and satellite models used in the N-body simulations. The first column specifies the component in question. The second column gives the density profile, either in spherical coordinates ( $r$ ), or cylindrical polar coordinates ( $R, z$ ). The values of the parameters of each profile are listed in column 3. The satellites are all described by King models (King 1966). For these we specify the core radius,  $r_c$ , and the concentration  $c = \log_{10} r_t/r_c$  where  $r_t$  is the tidal radius of the satellite. The final column lists the number of particles used to represent each component in the standard case.

Component	Density Profile	Parameters	Number of Particles
Halo	$\rho_H(r) = \frac{M_H \alpha}{2\pi^{3/2} r_{\text{cut}}} \frac{\exp(-r^2/r_{\text{cut}}^2)}{r^2 + \gamma^2}$	$M_H = 7.84 \times 10^{11} M_\odot$ $\gamma = 3.5 \text{kpc}$ $r_{\text{cut}} = 84 \text{kpc}$ $\alpha = 1.076$	171752
Disk	$\rho_D(R, z) = \frac{M_D}{4\pi R_D^2 z_0} \exp(-R/R_D) \text{sech}^2(z/z_0)$	$M_D = 5.6 \times 10^{10} M_\odot$ $R_D = 3.5 \text{kpc}$ $z_0 = 700 \text{pc}$	40960
Bulge	$\rho_B(r) = \frac{M_B}{2\pi} \frac{a}{r(a+r)^3}$	$M_B = 1.87 \times 10^{10} M_\odot$ $a = 525 \text{pc}$	4096
Satellite S1	King Model	$M_S = 5.60 \times 10^9 M_\odot$ $r_c = 1 \text{kpc}$ $c = 0.8$	8192
Satellite S2	King Model	$M_S = 5.60 \times 10^9 M_\odot$ $r_c = 500 \text{pc}$ $c = 1.1$	8192
Satellite S3	King Model	$M_S = 1.12 \times 10^{10} M_\odot$ $r_c = 875 \text{pc}$ $c = 1.0$	8192

**Table 2.** Properties and initial orbital parameters of the satellites in the N-body simulations. Column 2 specifies the satellite model used (as defined in 1). Column 3 lists  $\theta_i$ , the angle between the initial angular momentum vector of the satellite and that of the disk. Column 4 lists the circularity of the satellite's initial orbit,  $\epsilon_J$ , while column 5 lists the initial radial position of the satellite (which is the apocentre of its orbit),  $r_a$ . Column 6 specifies whether the simulation contains a disk or not (note that  $\theta_i$  is undefined for diskless simulations G2Sxx).

Model	Satellite	$\theta_i$	$\epsilon_J$	$r_a/\text{kpc}$	Disk?
G1S1	S1	45°	0.33	59.0	✓
G1S2	S1	0°	0.55	55.0	✓
G1S3	S1	45°	0.55	55.0	✓
G1S4	S1	90°	0.55	55.0	✓
G1S5	S1	135°	0.55	55.0	✓
G1S6	S1	180°	0.55	55.0	✓
G1S7	S1	0°	0.82	46.5	✓
G1S8	S1	45°	0.82	46.5	✓
G1S9	S2	0°	0.55	55.0	✓
G1S10	S2	45°	0.55	55.0	✓
G1S11	S2	90°	0.55	55.0	✓
G1S12	S2	135°	0.55	55.0	✓
G1S13	S2	180°	0.55	55.0	✓
G1S14	S3	45°	0.55	55.0	✓
G1S15	S3	135°	0.55	55.0	✓
G2S1	S1	N/A	0.33	59.0	✗
G2S2	S1	N/A	0.55	55.0	✗
G2S7	S1	N/A	0.82	46.5	✗
G2S9	S2	N/A	0.55	55.0	✗
G2S14	S3	N/A	0.55	55.0	✗

keeping the sum of the kinetic and potential energies constant. In the thin disk approximation, the total vertical energy per unit area of the disk  $e_z$  can be written as (TO)

$$e_z = t_z + w_{\text{dd}} + w_{\text{dh}}, \quad (3)$$

where all quantities are surface energy densities,  $t_z$  is the disk vertical kinetic energy,  $w_{\text{dd}}$  is the disk self-gravitational energy and  $w_{\text{dh}}$  is the gravitational energy due to the disk/halo interaction. The vertical energy  $e_z$  is defined to be zero in a state where the disk has zero thickness and zero vertical velocities. Expressions for  $t_z$ ,  $w_{\text{dd}}$  and  $w_{\text{dh}}$  are derived in Appendix C. Following TO, we assume virial equilibrium and find

$$2t_z - w_{\text{dd}} - 2w_{\text{dh}} = 0, \quad (4)$$

and so

$$e_z = \frac{3}{2}w_{\text{dd}} + 2w_{\text{dh}}. \quad (5)$$

The density for our model disks is proportional to  $\text{sech}^2 z/z_0$  in the vertical direction. For this density profile we find from eqn.(5) (TO)

$$e_z = \frac{3}{2}\pi G \Sigma_d^2(R) z_0 + \frac{\pi^2}{12} \Sigma_d(R) z_0^2 \frac{GM_h(R)}{R^3}, \quad (6)$$

where  $R$  is radius in the disk plane,  $\Sigma_d(R)$  is the disk surface mass density, and  $M_h(R)$  is the mass in the (spherical) halo plus bulge within radius  $R$ . Since the vertical kinetic energy per unit area is  $t_z = \frac{1}{2}\Sigma_d \sigma_z^2$ , we also find from eqn.(4)

$$\sigma_z^2 = \pi G \Sigma_d(R) z_0 + \frac{\pi^2}{12} GM_h(R) z_0^2 / R^3 \quad (7)$$

**Table 3.** Comparison of results from the analytic and N-body calculations of satellite evolution. Column 1 lists the model number, while column 2 lists the type of calculation (analytic or N-body). Column 3 gives the change in the disk vertical kinetic energy due to the satellite at the end of the simulation, both in absolute units and as a percentage of the initial disk vertical kinetic energy (values in parentheses). Where the analytic and N-body estimates of the disk energy differ by more than a factor of two we show the values in bold type. Columns 4 and 5 list the times at which the satellite reaches 50% and 10% of its initial mass respectively.

Model	Type	$\frac{\Delta T_z(4\text{Gyr})}{10^{14} M_{\odot} \text{km}^2 \text{s}^{-2}}$	$t_{50}/\text{Gyr}$	$t_{10}/\text{Gyr}$
G1S1	Analytic	<b>0.133</b> (25%)	1.24	2.01
G1S1	N-body	<b>0.048</b> (8%)	1.43	2.42
G1S2	Analytic	0.257 (49%)	1.51	2.89
G1S2	N-body	0.230 (40%)	1.80	2.09
G1S3	Analytic	0.184 (35%)	2.20	3.19
G1S3	N-body	0.164 (29%)	2.34	3.69
G1S4	Analytic	<b>0.029</b> (5%)	2.32	3.73
G1S4	N-body	<b>0.071</b> (12%)	2.74	> 4.00
G1S5	Analytic	<b>0.032</b> (6%)	2.24	3.77
G1S5	N-body	<b>0.074</b> (13%)	2.60	3.90
G1S6	Analytic	0.177 (33%)	1.94	3.00
G1S6	N-body	0.236 (41%)	2.16	3.16
G1S7	Analytic	<b>0.056</b> (11%)	2.70	> 4.00
G1S7	N-body	<b>0.252</b> (44%)	2.23	2.32
G1S8	Analytic	<b>0.096</b> (18%)	3.23	> 4.00
G1S8	N-body	<b>0.342</b> (60%)	3.59	3.95
G1S9	Analytic	0.272 (51%)	1.92	3.30
G1S9	N-body	0.258 (45%)	1.92	1.98
G1S10	Analytic	0.244 (46%)	2.53	3.28
G1S10	N-body	0.424 (74%)	3.22	3.47
G1S11	Analytic	<b>0.114</b> (22%)	2.86	3.59
G1S11	N-body	<b>0.252</b> (44%)	3.38	4.02
G1S12	Analytic	0.131 (25%)	2.89	3.58
G1S12	N-body	0.210 (37%)	3.43	> 4.00
G1S13	Analytic	0.507 (96%)	2.32	2.62
G1S13	N-body	0.457 (80%)	2.84	3.25
G1S14	Analytic	0.521 (98%)	1.58	2.52
G1S14	N-body	0.456 (80%)	1.60	1.85
G1S15	Analytic	0.438 (83%)	1.78	2.09
G1S15	N-body	0.253 (44%)	1.76	2.20

This expression is used to calculate the vertical velocity dispersion at each radius from the scaleheight  $z_0$ . <sup>†</sup>

<sup>†</sup> Note that here we differ slightly from VW by including the contribution of the halo gravity to the disk vertical velocity dispersion. This is typically a small, although not negligible, contribution over the bulk of the disk.

To relate the radially-dependent vertical energy per unit area to the global total vertical energy, we make the assumption that the disk scale height is constant with radius, since this is observed to be a good approximation for real galaxies (e.g. de Grijs & Peletier 1997). We can then integrate eqn.(6) over the whole disk to find the total vertical energy. Using  $\Sigma_d = (M_d/2\pi R_d^2) \exp(-R/R_d)$  for an exponential disk of radial scale-length  $R_d$  we find

$$E_z = \frac{3}{16} M_d V_d^2 h + \frac{\pi^2}{12} M_d V_d^2 h^2 \int_0^\infty \left[ \frac{V_h(R)}{V_d} \right]^2 \frac{\exp(-x)}{x} dx, \quad (8)$$

where the fractional scaleheight  $h = z_0/R_d$ ,  $V_d^2 = GM_d/R_d$  and  $V_h^2 = GM_h(R)/R$ . Integrating eqn.(7) gives a similar expression for the total vertical kinetic energy  $T_z$ . Once the total vertical energy  $E_z$  is known, the above equation is easily solved for  $h$  and hence  $z_0$ .

### 2.2.3 Local vs. Global Heating

In §2.2.2 we made the assumption that the energy deposited in the disk by satellites was distributed throughout the disk in such a way as to produce a scale-height that was independent of radius. However, the increase in energy per unit mass caused by a satellite passing through the disk will initially be greatest close to the point of impact. Since satellite encounters frequently trigger global modes of the disk it is not implausible that this energy becomes quickly redistributed throughout the disk. However, it is interesting to consider the opposite extreme in which energy is deposited at the position of the satellite and remains there. We refer to these two extremes as “global” and “local” heating. To study local heating we accumulate the energy deposited by satellites in a narrow annulus of the disk (in practice we use a Gaussian window function), centred on the disk half-mass radius. We then assume that the specific energy of disk material is proportional to the same window function and use the relations of §2.2.2 to compute the resulting scaleheight at the half-mass radius.

Observations of real galactic disks (de Grijs & Peletier 1997) indicate that the scale height is reasonably constant with radius, at least for late-type galaxies. For this reason we prefer the global heating assumption, but consider local heating also as an interesting comparison.

### 2.2.4 Further Aspects

Below we detail how we deal with energy<sup>‡</sup> deposited in a gaseous disk and how we treat galaxy mergers, gas accretion and star formation.

*Gas in Galaxy Disks:* Disks in our model in general consist of both stars and gas. We assume that gas and stars in the disk are heated at the same rate per unit mass, but assume that the gas dissipates this energy rapidly, such that energy deposited in the gas is effectively lost.

*Gas Accretion and Star Formation:* Gas accreted onto

<sup>‡</sup> For convenience, we use the expression “energy” to imply “disk vertical energy” from here on, unless explicitly stated otherwise.

the disk is assumed to initially have zero energy. When gas turns into stars therefore, these stars start out with zero energy. We will assume that these new stars rapidly mix with the pre-existing stellar population such that all stars have the same energy.

*Gas in Scale Height Calculation:* When calculating the disk scale-height the mass of gas in the disk is always included in the disk potential.

*Galaxy Mergers:* In a major merger all disks are destroyed, and so we zero the energy of the resulting galaxy. In minor mergers stars from the satellite galaxy disk and bulge are added to the bulge of the central galaxy. In this case, the energy of the satellite disk is lost, while that of the central galaxy disk is unchanged.

### 2.2.5 Heating of Disks by Scattering by Clouds

Substructure in the halo is not the only source of heating for disks. Two other plausible mechanisms for disk heating are gravitational scattering of stars by massive gas clouds (Spitzer & Schwarzschild 1953; Lacey 1984) and scattering of stars by spiral arms (Carlberg & Sellwood 1985). The latter mechanism has difficulty in producing any heating in the vertical direction, so we will focus on the first mechanism. Lacey (1984) derived expressions for the rate at which scattering by clouds increases the vertical and horizontal epicyclic energies of the stars. In general, these expressions depend on both  $\sigma_R$  and  $\sigma_z$ , but acting by themselves the clouds tend to drive the ratio  $\sigma_z/\sigma_R$  to an equilibrium value. We calculate the rate of increase of vertical energy per unit mass for the stars  $\varepsilon_z$  using Lacey's eqn.(39), evaluated for the equilibrium  $\sigma_z/\sigma_R$  and in the limit that the scaleheight of the stars is larger than that of the clouds. This gives

$$\left(\frac{d\varepsilon_z}{dt}\right)_{\text{clouds}} = \frac{2G^2 \Sigma_c M_c \ln \Lambda_c \nu}{\sigma_z^2} \alpha_s^3(\beta) K_s(\beta) \quad (9)$$

where  $\Sigma_c$  is the surface density in clouds,  $M_c$  is the cloud mass,  $\ln \Lambda_c$  is the Coulomb logarithm for scattering of stars by clouds and  $\nu$  is the vertical epicyclic frequency.  $\alpha_s(\beta)$  and  $K_s(\beta)$  are functions of  $\beta = 2\Omega/\kappa$  which are tabulated by Lacey,  $\Omega$  being the angular velocity for circular orbits and  $\kappa$  the radial epicyclic frequency. We obtain the total contribution of scattering by clouds to the increase of vertical energy by integrating eqn.(9) over radius:

$$\dot{E}_{z,\text{clouds}} = \int_0^\infty \Sigma_d \left(\frac{d\varepsilon_z}{dt}\right)_{\text{clouds}} 2\pi R dR \quad (10)$$

Numerical simulations of heating by clouds agree fairly well with the analytically-predicted velocity dependence ( $d\sigma^2/dt \propto \sigma^{-2}$ ), but have given somewhat conflicting results about the amplitude of the effect; Villumsen (1985) found heating rates  $d\sigma^2/dt$  at a given  $\sigma$  about 6 times lower than the analytical prediction, while Hanninen & Flynn (2002) found rates 3–8 times higher.

Our galaxy formation model predicts the total mass of gas in the disk of each galaxy as a function of time. We assume that the gas is distributed radially in the same way as the stars, with a constant fraction being in the form of giant molecular clouds. For our standard case we will assume that

25% of the gaseous mass of the disk is in clouds (Granato et al. 2000), that they have mass-weighted mean mass of  $M_c = 6.6 \times 10^5 M_\odot$  (Lacey 1984) and typical radius  $a_c = 16\text{pc}$  (Granato et al. 2000), and that  $\beta = 1.5$ . For each model galaxy, we integrate the heating due to scattering from molecular clouds over each timestep in the calculations, and add this to that which arises from interactions with satellites.

## 3 CALIBRATION USING N-BODY SIMULATIONS

As has been noted by several authors, the amount of heating caused by a given satellite is difficult to determine analytically since some of the energy may drive global perturbations (e.g. warps) in the disk, and satellites may trigger bar instabilities leading to an enhanced heating rate. Furthermore, our approach to dynamical friction from the disk follows the methods of Chandrasekhar (e.g. Binney & Tremaine 1987, section 7.1), which assume that each particle interacts with the satellite only once. If the satellite orbital period is close to the rotation period of the disk however (or to some other resonance of the disk orbits), this assumption fails. Instead, a single particle may interact with the satellite multiple times on consecutive orbits. This problem should therefore ideally be approached in terms of resonant interactions between satellite and disk (Goldreich & Tremaine 1979; Donner & Sundelius 1993; Wahde, Donner & Sundelius 1996; Weinberg & Katz 2002). We retain the Chandrasekhar methods for their simplicity, and will show that they provide a reasonable approximation to the dynamical friction due to disks in the regimes of interest.

### 3.1 N-body Simulations

We begin by testing and calibrating our analytic calculations against numerical simulations of disk heating. In principle, the simulations of VW are ideal for this purpose. However, the central densities and velocity dispersions for the King model satellites given by VW appear to be incorrect, in the sense of being too low for the reported concentration parameters. This seems to have made the satellites in their simulations too weakly bound. It is unclear a priori how this affects their results. We have therefore decided to repeat their calculations. This has two other advantages:

- We can repeat each simulation without the disk component, allowing us to constrain the halo and disk dynamical friction components of our model separately.
- We can perform convergence tests by increasing the number of particles in the simulation to ensure that disk heating is being estimated accurately by the simulations.

We carry out the same set of simulations as VW. Briefly, each simulation consists of a galaxy consisting of a bulge, disk and dark matter halo, plus a satellite object. Density profiles and the number of particles used for each component are listed in Table 1, while other details of each simulation (type of satellite used, initial satellite orbital parameters and whether or not a disk is included) are listed

in Table 2. Initial conditions are created using the techniques of Hernquist (1993). The galaxy and satellite are then evolved separately, as described by VW, using the GADGET code (Springel, Yoshida & White 2001) to allow them to reach equilibrium. We employ GADGET's new cell-opening criterion for tree walks (`TypeOfOpeningCriteria=1`) with an accuracy of `ErrTolForceAcc=0.001`, together with `TypeOfTimestepCriterion=1` with `ErrTolVelScale=10.0`. GADGET uses adaptive time-stepping. We impose no minimum timestep size, but impose a maximum size of `MaxSizeTimestep=0.01` (in GADGET's default internal units). All particles in the simulation are given a softening length of 0.175kpc. With these choices energy is conserved to better than 1% throughout the simulations. The two sets of initial conditions are then superimposed and evolved for 4Gyr.

These simulations are labelled G1S1 to G1S15 as in VW. We also perform a simulation with no satellite, G1S0, to measure the two-body heating rate in the disk. We repeat each simulation without a disk component, labelling these G2S1 to G2S15 (note that, due to the lack of a disk component, only models G2S1, G2S2, G2S7, G2S9 and G2S14 are unique). We also repeated two of the runs with double and quadruple the number of particles, in order to test how well the results have converged. The convergence tests are described in Appendix D. They indicate that the convergence is good for the evolution of the mass and orbit of the satellite, and adequate for the increase in the vertical energy of the disk.

Each simulation output is analyzed in order to determine the position, velocity and mass of the satellite (computed for those particles which remain bound to the satellite), and the vertical kinetic energy of the disk. We determine which particles are bound to the satellite using the following algorithm:

- (i) Begin by considering all the satellite particles that were bound to the satellite at the previous timestep (or simply use all satellite particles for the first timestep).
- (ii) Compute the mean position and velocity, and the mass of the satellite from these particles.
- (iii) For each particle in this set, determine if it is gravitationally bound to the other particles in the set.
- (iv) Retain only those particles which are bound and go back to step 2. Repeat until the mass of the satellite converges.

To determine the vertical kinetic energy of the disk  $T_z$  at each output time, we first locate the centre of the disk and its mean velocity (since the satellite mass is comparable to that of the disk, the disk moves around significantly as the satellite passes by). We then rotate to the frame defined by the principal axes of the disk inertia tensor, and sum the kinetic energies of particles in the direction defined by the shortest axis (which corresponds to the  $z$ -axis for an untilted disk). This rotation is necessary because the disk can become tilted through its interaction with the satellite (as also noted by VW). If we did not rotate the frame, then pure circular motions in a tilted disk would appear as vertical energy in the original unrotated frame.

One final step is necessary in order to obtain the *increase* in the disk vertical energy due to the interaction with the satellite. Even in the absence of a satellite, the vertical kinetic energy of the disk increases in the simulation due to numerical relaxation (mainly two-body scattering), from  $0.57 \times 10^{14} M_{\odot} \text{km}^2 \text{s}^{-2}$  at  $t = 0$  to  $0.81 \times 10^{14} M_{\odot} \text{km}^2 \text{s}^{-2}$  at  $t = 4\text{Gyr}$ , for our standard particle number. This increase of  $0.24 \times 10^{14} M_{\odot} \text{km}^2 \text{s}^{-2}$  due to two-body relaxation is larger than the heating by the satellite in many of the cases run. Therefore to obtain the increase in vertical energy due to the satellite at time  $t$ , which we denote as  $\Delta T_z(t)$ , we subtract off the energy of the unperturbed disk (from model G1S0) at the same time  $t$ . Based on runs of model G1S0 with different random number seeds but the same number of particles, the increase in  $T_z$  due to numerical relaxation is determined to an accuracy of  $(0.02 - 0.03) \times 10^{14} M_{\odot} \text{km}^2 \text{s}^{-2}$  in the standard case, so the uncertainty in  $\Delta T_z$  introduced by the subtraction is small compared to  $\Delta T_z$  itself.

### 3.2 Comparison with Analytic Calculations

To constrain the parameters of our analytic model of satellite orbits, we mimic each N-body simulation using the analytic techniques. For the purposes of this comparison, we use density profiles for host and satellite systems identical to those of the N-body simulations. Taylor & Babul (2001) compared their model of satellite galaxy orbits to the orbital radii and satellite masses as a function of time from the simulations of VW, finding generally good agreement. We repeat their analysis here, using our own model of satellite dynamics, but extend it to include the calculation of disk heating. We will use this comparison to fix the four free parameters of our satellite orbit model,  $f_{\text{orb}}$ ,  $f_{\Lambda,h}$ ,  $f_{\Lambda,d}$  and  $\epsilon_h$ . As described in Appendix A,  $f_{\text{orb}}$  controls the timescale on which tidally stripped mass is actually lost from the satellite, while  $f_{\Lambda,h}$  and  $f_{\Lambda,d}$  appear in the Coulomb logarithms  $\Lambda_h$  and  $\Lambda_d$  for the dynamical friction force due to the halo and disk respectively. The parameter  $\epsilon_h$  controls the strength of gravitational shock heating and is defined in Benson et al. (2002a).

Using our satellite orbit model, each orbit is evolved for 4 Gyr. Figures 2 and 3 show the orbital position and velocity and the remaining bound mass and orbital energy of the satellite for models G2S2 and G1S3 respectively, with our N-body results shown as open circles. Figure 3 also shows the energy deposited in the disk for model G1S3. Specifically, we show the vertical kinetic energy of the simulated disk after subtraction of the vertical kinetic energy of the disk from model G1S0. Since model G1S0 contains no satellite, this approach removes both the initial energy of the disk, and the energy gained due to two-body relaxation during the simulation. We indicate at the top of each figure the satellite model used, the initial inclination of the orbit with respect to the galaxy disk ( $\theta_i$ ), the initial circularity ( $\epsilon_J$ ), the angular momentum of the satellite divided by the angular momentum of a circular orbit with the same energy) and the initial apocentric distance of the orbit ( $r_a$ ). Where they are available we show the results of VW as triangles. Note that in the simulation of VW the satellite loses mass more rapidly, due

to the incorrect profile it was given. For comparison we show as dashed lines the orbital radius and remaining bound mass from the analytic calculations of Taylor & Babul (2001) for this same model.

The results in Figs. 2 and 3 are for the parameter combination  $(f_{\text{orb}}, f_{\Lambda,h}, f_{\Lambda,d}, \epsilon_h) = (2.5, 1.5, 3.0, 1.0)$ . The values of  $f_{\text{orb}}$  and  $\epsilon_h$  are fixed by matching the mass loss rates found in the simulations with no disk component. The value of  $f_{\Lambda,h}$ , which controls the strength of the dynamical friction force due to the halo, is fixed by matching the rates of decay of the orbital radius in models with no disk component (such that the orbital decay is caused entirely by the halo plus bulge system). Finally,  $f_{\Lambda,d}$  is fixed by matching the rate of orbital decay in the models which include a disk component, for which the contribution of the disk to the dynamical friction force often dominates during much of the evolution. We have selected values which produce the best agreement with the set of fifteen models which were simulated. We find generally quite good agreement with the numerical results, comparable to that achieved by Taylor & Babul (2001)<sup>§</sup>. Recall that our model uses more general expressions for  $\Lambda_h$  and  $\Lambda_d$  than that of Taylor & Babul (2001). If we treat those numbers as free parameters (instead of  $f_{\Lambda,h}$  and  $f_{\Lambda,d}$ ) we are able to achieve even better agreement with the numerical simulations. However, our approach has the advantage that  $\Lambda_d$  and  $\Lambda_h$  scale in a physically reasonable way when we apply our model to very different satellite/host systems. In any case, orbital positions and velocities are typically matched accurately until the final merging of the satellite (where it becomes difficult to accurately determine these quantities in the N-body simulations). The satellite mass as a function of time is typically matched to within about 30–40%. Table 3 lists several results (the final change in the disk energy and the times at which the satellite reaches 50% and 10% of its original mass) from both analytic and N-body calculations for comparison.

It is worth noting that the free parameters of our orbit model are set without reference to the rate of disk heating seen in the numerical simulations. Thus, the heating rates we predict are entirely specified by other considerations. The lower right-hand panel in Fig. 3 shows the disk vertical kinetic energy from our analytic model and from the N-body simulation (we infer the vertical kinetic energy in our analytic model from the known total energy as described in §2.2.2). We find that our analytic model reproduces the disk energy measured at the end-points of the numerical simulations to within a factor of two in nine out of the fifteen simulations carried out (see Table 3). Of the six models which do not achieve this level of agreement, one (G1S7) has the satellite orbit prograde in the disk plane ( $\theta_i = 0^\circ$ ), two (G1S4 and G1S11) have polar orbits  $\theta_i = 90^\circ$ , two (G1S1 and G1S8) are on inclined prograde orbits  $\theta_i = 45^\circ$ , and one (G1S5) on an inclined retrograde orbits  $\theta_i = 135^\circ$ .

Of the three out of the six discrepant cases on inclined

<sup>§</sup> It should be noted that Taylor & Babul (2001) were attempting to match the simulations of VW, rather than our simulations, so that one should not expect exact agreement of their results with ours.

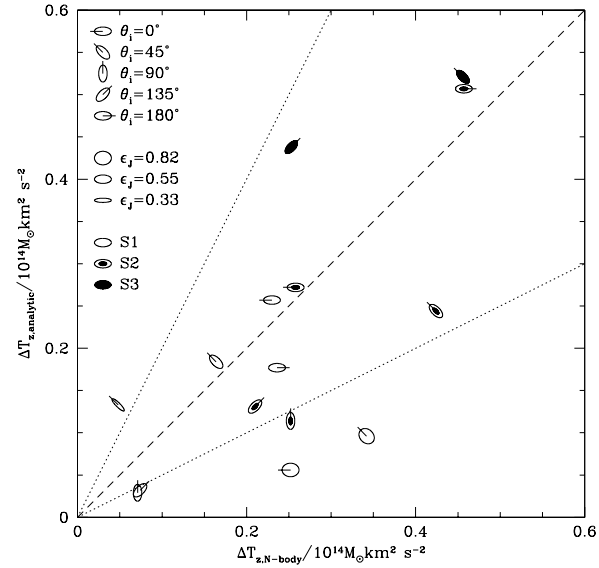


**Figure 4.** A comparison between the change in the vertical component of the disk kinetic energy,  $\Delta T_z$ , predicted by analytic and N-body models. The dashed line is the locus of perfect agreement between the two, with the two dotted lines indicating factor of two discrepancies. The symbols, one for each of the fifteen simulations G1S1 to G1S15, also indicate through their orientation, shape and shading the orbital inclination, the orbital circularity and the the satellite model respectively.

orbits, in two (G1S5 and G1S8) the analytic model under-predicts the N-body heating by factors of 2–4, while in the other case (G1S1) the analytic model over-predicts the N-body heating by around a factor 3. Inaccuracies in the determination of the disk inclination may explain the failures of models G1S5 and G1S8, but this cannot be true for model G1S1 (since an inaccurate determination of the disk inclination always increases the measured disk energy).

For model G1S7 (the prograde orbit in the disk plane) the dynamical friction force from the disk is overestimated in the analytical model relative to the N-body simulation, resulting in the satellite becoming trapped in an orbit rotating with the disk. This results in there being no energy transfer to the disk at later times, so that the analytic model underestimates the heating by a factor of 4.5. For the polar orbits G1S4 and G1S11, mass loss in the analytic model is too rapid, again reducing the heating rate compared to the N-body calculation. Consequently, these two models under-predict the N-body heating by just over a factor 2.

Figure 4 shows the N-body and analytic model results for the disk kinetic energy in a graphical way. We plot  $\Delta T_z$  for the analytic model versus that for the N-body model. The dashed line is the locus of perfect agreement between the two, with the two dotted lines indicating factor of two discrepancies. The symbols, one for each of the fifteen simulations G1S1 to G1S15, also indicate through their orientation, shape and shading the orbital inclination, the orbital circularity and the the satellite model respectively (as described by the key in the figure).

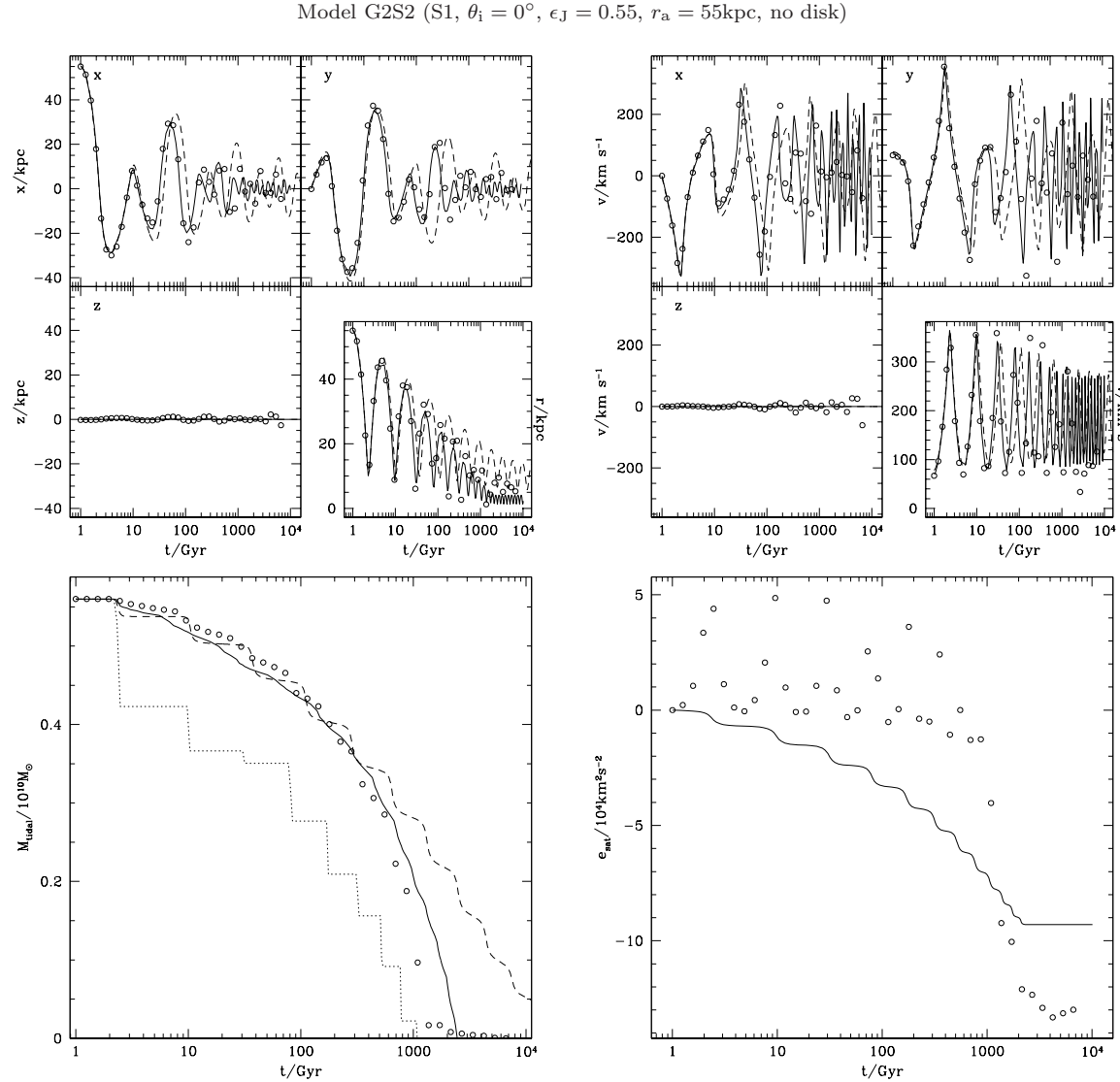


**Figure 2.** Evolution of the satellite and its orbit in the diskless model G2S2. We compare the results from our analytical model (solid lines) with the analytical model of Taylor & Babul (2001) (dashed lines) and with our N-body simulation (circles). *Top left-hand panel:* The orbital position and radius of the satellite as a function of time. *Top right-hand panel:* The orbital velocity of the satellite and its components as a function of time. *Lower left-hand panel:* The remaining bound mass of the satellite as a function of time. The dotted line shows the mass of the satellite if mass loss beyond the tidal radius occurs instantaneously (i.e.  $f_{\text{orb}} = 0$ ). *Lower right-hand panel:* The change in the specific orbital energy of the satellite as a function of time.

Several of the N-body simulations show evidence of bar formation in the central regions of the disk. This is particularly evident for satellites on prograde orbits in the disk plane. Bars may be expected to enhance the transfer of energy to the disk, and may be part of the reason why the analytic model (which does not allow for bar formation) substantially underpredicts the amount of heating in some cases (e.g. G1S5 and G1S7, of which the latter shows a particularly strong bar in the N-body simulation).

The efficiency of vertical heating,  $\epsilon_z$ , is an important component of our calculations. If we did not include this efficiency the predicted heating rates would be up to 4 times higher (depending on the particular orbit under consideration—the effect is largest for near-circular prograde

orbits in the disk plane and polar orbits), with a factor of 3 being more typical.

The inclusion of the  $\theta$  dependence in the expression for  $\Lambda_d$  (see Appendix B2.2) tends to reduce the heating rate slightly. The effect is only minor for most orbits, but is of greater importance for orbits in the disk plane, helping to improve the agreement with the simulation results in those cases. The use of an anisotropic disk velocity dispersion in the dynamical friction force typically has an even smaller effect on the rate of disk heating, typically increasing the rate by a few percent (although in some cases the rate is decreased by an equally small amount). Prograde orbits in the disk plane are, once again, most strongly affected, with heating rates being reduced by 20–40%

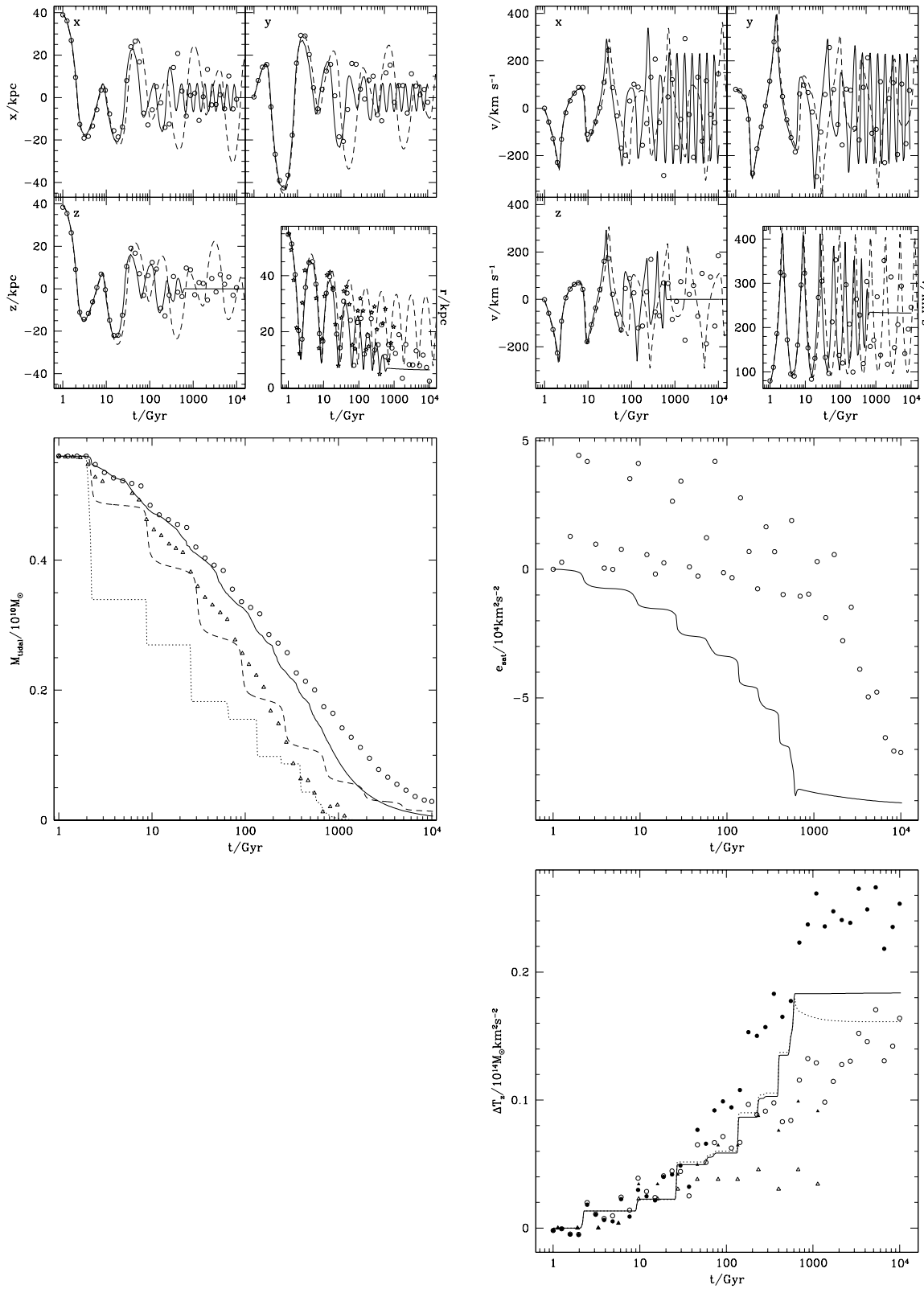
Model G1S3 (S1,  $\theta_i = 45^\circ$ ,  $\epsilon_J = 0.55$ ,  $r_a = 55\text{kpc}$ )

Figure 3.

**Figure 3.** (cont.) Properties of the orbiting satellite and host halo galaxy disk in model G1S3. We compare the results from our analytic calculations (solid lines) and those of Taylor & Babul (2001) (dashed lines), and from our N-body simulation (circles) and that of Velázquez & White (1999) (triangles). *Top left-hand panel:* The orbital position and radius of the satellite as a function of time. *Top right-hand panel:* The orbital velocity and speed of the satellite as a function of time. *Centre left-hand panel:* The remaining bound mass of the satellite as a function of time. The dotted line shows the mass of the satellite if mass loss beyond the tidal radius occurs instantaneously. *Centre right-hand panel:* The change in specific orbital energy of the satellite with time. *Lower right-hand panel:* The vertical kinetic energy of the central galaxy disk. Filled symbols show the energy measured in the original coordinate frame of the disk. Open symbols show the energy measured in a frame coinciding with the principal axes of the disk inertia tensor at each point in time. The dotted line shows the result obtained if the energies of the disk in each direction ( $R, \phi, z$ ) are assumed to reach equipartition.

The N-body model galaxy contains a bulge with mass 1/3 that of the disk. VW also performed simulations with bulges of mass 1/5 and 2/3 that of the disk to examine the influence of the bulge on the heating rate, finding that a more massive bulge reduced the amount of disk heating. Our analytical model typically reproduces this trend, with approximately the same strength.

To summarize, we are able to reproduce the rates of disk heating seen in numerical simulations for the majority of the cases considered. Where the analytic approach “fails” (we say “fails”, since the N-body techniques have their own inadequacies and do not represent the absolute truth), the orbit is often found to be an inclined orbit. In the other cases the incorrect heating rate is a consequence of an incorrect estimate of the disk dynamical friction force or tidal mass loss rate. In these cases we find that the heating rate is underestimated by a factor 3 on average. It is worth emphasizing that our analytic calculation produces several of the trends observed in the N-body heating rates. For example:

- heating is greatly suppressed for satellites on polar orbits;
- differences between heating rates for pro- and retrograde orbits (which are not always in the same sense—different types of satellite give different results) are reproduced
- differences due to the concentration or initial mass of the satellite are clearly reproduced.

The trend of increased heating for more circular orbits (as seen in the N-body simulations) is not reproduced however.

While it is clear that the analytic model is not perfect at reproducing the N-body heating rates, it does as well as the N-body simulations in the majority of cases, i.e. it is as accurate as our convergence tests imply the N-body results themselves are. In other cases it still provides a reasonable approximation.

## 4 RESULTS

### 4.1 Scaleheight Distribution for Disk Galaxies

Having demonstrated that our model is able to calculate disk heating rates with reasonable accuracy, we proceed to apply these calculations to galaxy formation in a cosmological setting. Specifically, we implement this model of disk heating in the GALFORM semi-analytic model of galaxy formation described by Cole et al. (2000) and Benson et al. (2002a), based on a standard  $\Lambda$ CDM cosmology with  $\Omega_0 = 0.3$  and

$\Lambda_0 = 0.7$ <sup>¶</sup>. This model follows the growth of galactic disks in a merging hierarchy of dark matter halos. At each point in time the model predicts the mass and radial size of the galactic disk present at the centre of each halo. It also predicts the rate at which sub-halos are merging into each halo, which we take as input for our calculations of satellite evolution and disk heating. We assume that only direct progenitors of the halo cause heating (i.e. sub-halos are able to heat the disk of the galaxy, but sub-sub-halos are not considered). This is to avoid double-counting of mass. We will consider briefly below the effect of allowing all progenitors to heat disks.

Using this model, we generate a representative sample of galaxies living in dark matter halos spanning a wide range of masses. For each galaxy the model computes the usual properties predicted by this type of modeling (e.g. masses, luminosities etc.—see Cole et al. 2000), and now also predicts the vertical scale height of the galactic disk. Figures 5 and 6 show the resulting distribution of disk scale-heights, expressed in units of the disk radial scale-length, for galaxies with  $M_B - 5 \log h \leq -19.5$  (corresponding approximately to  $L_*$  and brighter galaxies) and  $-19.5 < M_B - 5 \log h \leq -17.0$  respectively. We include only spiral galaxies (which we define as any galaxy with a bulge-to-total ratio measured in dust-extinguished B-band light less than 0.4).

We remind the reader that we define the dimensionless scaleheight  $h = z_0/R_d$  in terms of the thickness parameter  $z_0$  in the  $\text{sech}^2$  vertical density law and the radial exponential scalelength  $R_d$ . The disk thickness can be equivalently defined as  $z_0 = \Sigma/(2\rho_0)$ ,  $\Sigma$  being the disk surface density and  $\rho_0$  the density at the midplane. However, many authors prefer to use the *exponential scaleheight* as their measure of the disk thickness. Since  $\text{sech}^2(z/z_0) \propto \exp(-2z/z_0)$  for  $z \gg z_0$ , the exponential scaleheight that would be measured for our assumed vertical profile is  $h_z = z_0/2$ .

The left and right-hand panels in Figures 5 and 6 show the scaleheight distributions for the global and local heating assumptions, from which we see that the results are not very sensitive to this choice. The figures also show the sensitivity of the results to two other parameters, one numerical and the other physical.

The numerical parameter concerns the galactocentric radius at which the satellite is assumed to merge with the main galaxy and stop heating the disk. In Cole et al. (2000) and in Paper I, we assumed that two galaxies merge at the

<sup>¶</sup> Benson et al. (2002c) describe small changes in the parameters of this model, relative to those of Benson et al. (2002a), which we retain here.

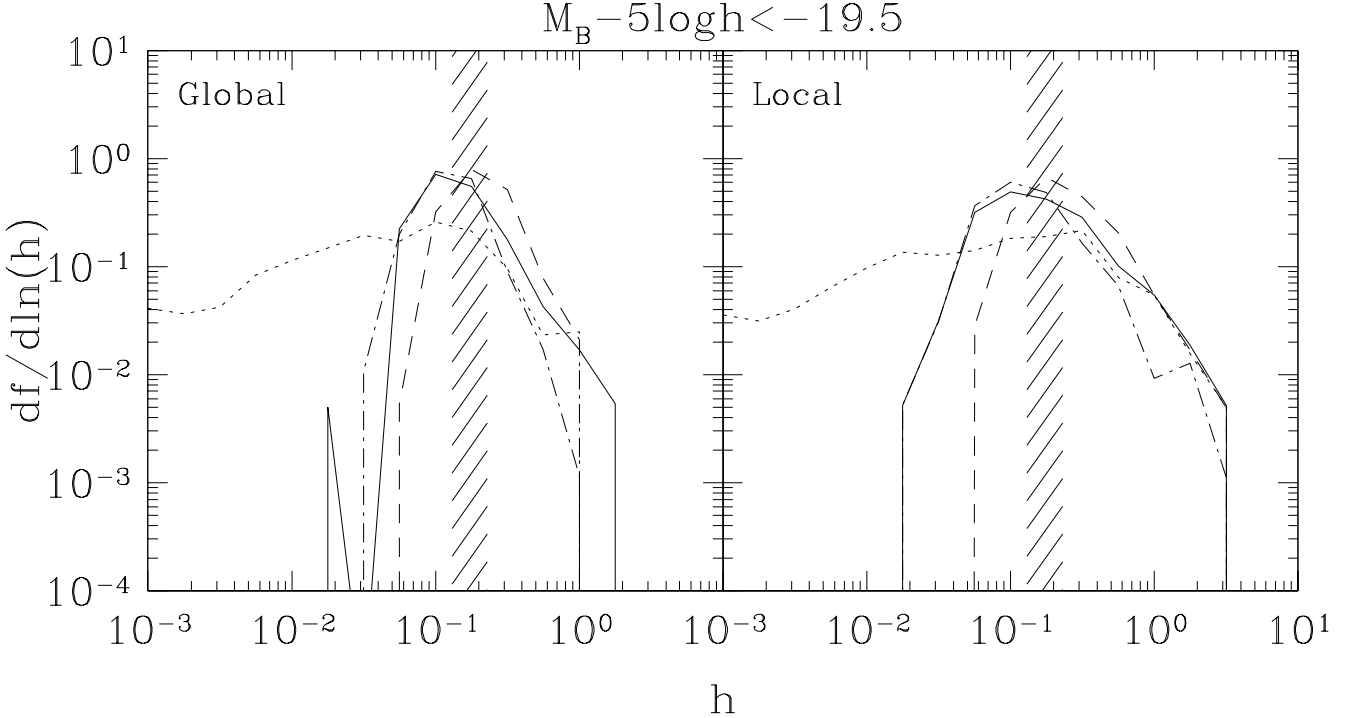


**Figure 5.** Normalized disk scale-height distributions for spiral galaxies with  $M_B - 5 \log h \leq -19.5$ . Left and right-hand panels show results for global and local heating respectively. Solid lines show results from our full calculation, including heating from substructure and from scattering by molecular clouds. The dotted line ignores the molecular cloud heating, while the dashed line increases the masses of individual clouds and the total mass in clouds by a factor of two over our standard values. These results correspond to satellite orbits which are integrated until they reach a radius  $(R_{\frac{1}{2}\text{sat}} + R_{\frac{1}{2}\text{host}})/8$ . For comparison, the dot-dashed line shows the result when the integration is stopped when a radius  $(R_{\frac{1}{2}\text{sat}} + R_{\frac{1}{2}\text{host}})$  is reached. The vertical shaded strip shows the observationally estimated scaleheight for the Milky Way galaxy, discussed in §4.4.

time when the separation of their centres  $R$  equals the sum of their half-mass radii,  $R_{\frac{1}{2}\text{sat}} + R_{\frac{1}{2}\text{host}}$ . However, once we include tidal stripping, it would seem reasonable to allow the satellite to sink down to  $R = 0$  and continue heating the disk while it does so. However, for numerical reasons we cannot integrate the satellite orbits down to  $R = 0$ . We have therefore calculated the disk heating when the satellite orbit is followed down to  $R = f_{\text{heat}}(R_{\frac{1}{2}\text{sat}} + R_{\frac{1}{2}\text{host}})$  for  $f_{\text{heat}} = 1, \frac{1}{2}, \frac{1}{4}$  and  $\frac{1}{8}$ . We find that the distribution of scaleheights has converged for  $f_{\text{heat}} = \frac{1}{8}$ , and use this as our standard value in what follows. We show in Fig. 5 results for  $f_{\text{heat}} = 1$  as the dot-dashed lines and  $f_{\text{heat}} = \frac{1}{8}$  as the solid lines, in both cases with disk heating by molecular clouds also included. We see that the differences in the scaleheight distribution are fairly small (they are somewhat more significant if we do not include disk heating by molecular clouds).

The physical parameter concerns the heating of the disk due to scattering of stars by giant molecular clouds, computed using eqn. (9). Our standard calculation, shown by the solid lines in Figs. 5 and 6, includes heating by the clouds with the parameters described in §2.2.5. The figures also show the results when no clouds are present (dotted lines) and when the masses of individual clouds and the fraction of gas in clouds are both doubled (dashed lines). Removing

clouds entirely results in a tail to very low  $h$  in our height distributions. These galaxies experienced very little heating due to substructure, and so their thickness was almost entirely due to heating by molecular cloud scattering. The peak of the distribution is little changed, but the median scaleheight is significantly reduced (see Figure 7). Doubling the cloud mass (dashed lines) results in a shift to somewhat thicker disks without changing the shape of the distribution.

It should be noted that the tails of our distributions extend to  $h > 1$ , which is clearly unphysical. Our analytical calculation uses the thin disk approximation  $h \ll 1$ , and so breaks down when  $h \sim 1$ . We interpret these objects as being disks which have been heated so much that they are no longer disks, and must instead resemble a spheroidal or irregular galaxy. For these galaxies our calculations have clearly broken down, but we can safely assume that they are no longer recognizable disk galaxies.

#### 4.2 Other Effects on the Scaleheight Distribution

Below we discuss tests of various potential systematic effects in our calculations.

*Merger Tree Resolution:* In our calculations we typically resolve dark matter substructures with masses greater than

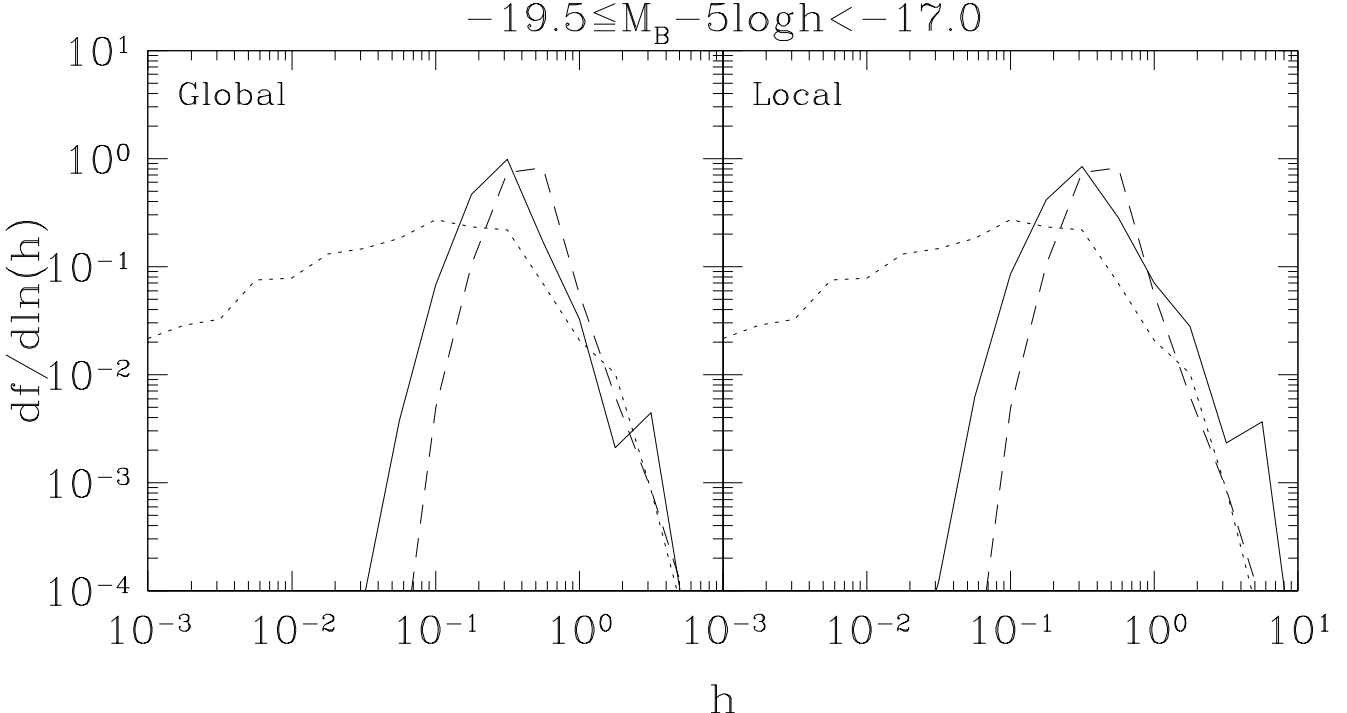


**Figure 6.** Normalized disk scale-height distributions for spiral galaxies with  $-19.5 < M_B - 5 \log h \leq -17.0$ . Left and right-hand panels show results for global and local heating respectively. Solid lines show results from our full calculation, including heating from substructure and from scattering by molecular clouds. The dotted line ignores the molecular cloud heating, while the dashed line increases the masses of individual clouds and the total mass in clouds by a factor of two over our standard values.

$5 \times 10^9 h^{-1} M_\odot$  in every merger tree. Thus, we do not account for the heating due to lower mass halos. Increasing the resolution of our calculations to  $10^9 h^{-1} M_\odot$  results in no significant increase in the amount of heating experienced by galaxies, indicating that our resolution is sufficient to estimate the total heating rate. (Note that the heating due to a satellite of mass  $M$  should scale approximately as  $M^2$ , making it relatively easy to achieve convergence here provided the number of satellites  $dN/d \ln M$  varies with mass less steeply than  $M^{-2}$  at small mass. In fact, numerical simulations indicate  $dN/d \ln M \sim M^{-0.8}$  for subhalos.)

*Effects of Sub-sub-halos:* In our standard calculation sub-sub-halos (i.e. halos which resided inside a larger halo which subsequently fell into a yet larger halo) do not contribute to the heating of disks. (Note however that this differs from the way in which we treat galaxy mergers in our calculations, where merging times of sub-sub-halos are computed from their own properties, not those of the sub-halo in which they reside.) An alternative approach would be to treat sub-sub-halos (and higher levels of the merging hierarchy) on an equal basis with sub-halos. To avoid double-counting of mass in this case, we remove the mass bound into sub-sub-halos when determining the mass of a sub-halo. The density profile of the sub-halo is then scaled down to remove this same amount of mass before computing heating rates.

If we adopt this approach we find that the distribution of scale heights is shifted to slightly larger values. It should

be noted that heating by sub-sub-halos would only be important if sub-sub-halos can survive after the sub-halo in which they live is tidally destroyed. While it is unlikely that this occurs to any great extent, numerical simulations could in principle answer this question.

*Effect of Cosmological Model:* Finally, we have repeated our calculations in an  $\Omega_0 = 1$  cosmology, using the  $\tau$ CDM parameter set used by Benson et al. (2000a), but including the effects of photoionization suppression<sup>||</sup>. This model is not as successful at matching the properties of  $z = 0$  galaxies as our standard  $\Lambda$ CDM model, in particular galaxies are somewhat too faint to match the observed luminosity function (by about 0.75 magnitudes in the B-band), forcing us to adopt an unphysical value of  $\Upsilon$  (the mass-to-light ratio normalization parameter) of 0.7. We find that the median scaleheight for  $L_*$  disk galaxies is slightly smaller in this model than in our  $\Lambda$ CDM model. At first sight this seems surprising, since, as noted by TO, there is more infall of substructure at late times in an  $\Omega_0 = 1$  cosmology, which results in a larger rate of heating at the present day. How-

<sup>||</sup> Note that Benson et al. (2000a) adopted an unphysically high merger rate in order to produce a good match to the galaxy luminosity functions. With our more detailed model of merging we no longer have the freedom to adjust the merger rate in this way. We find that, in this cosmology, our revised merger model produces somewhat too few elliptical galaxies.

ever, our model galaxies in this cosmology are younger than their  $\Lambda$ CDM counterparts (due to the later growth of structure and to the stronger feedback we must adopt in this model), which means they have less time in which to be heated. These two effects counteract each other.

We can understand this in more detail by examining the growth histories of the dark matter halos hosting  $L_*$  spiral galaxies. In our model, halos of present-day mass  $2 \times 10^{12} h^{-1} M_\odot$  have on average assembled half of their mass by redshifts of 0.45 and 0.91 respectively in the  $\tau$ CDM and  $\Lambda$ CDM cosmologies. The mean stellar ages for  $L_*$  disk galaxies reflect this difference in halo assembly epoch, being 4.0 and 5.5Gyr for  $\tau$ CDM and  $\Lambda$ CDM. We find that the host halos on average accrete close to 25% of their total mass over these galaxy lifetimes in both cosmologies. Therefore the number of substructures infalling onto a galaxy over its lifetime should be roughly the same in both cosmologies, consistent with the similar disk scale height distributions mentioned above. It should be kept in mind that the disks in our  $\Omega_0 = 1$  model are unrealistic (e.g. they are too low in luminosity for a reasonable  $\Upsilon$  and, more importantly, too young). An  $\Omega_0 = 1$  model which produced realistic disks might predict larger (or smaller) scale-heights. The important lesson is that disk scaleheights depend on the details of galaxy formation as well as on the cosmological model.

### 4.3 Scale Heights as a Function of Luminosity

In Fig. 7 we show the median value of  $h$  as a function of absolute magnitude for spiral galaxies in our standard model. The squares show the results for heating by substructure alone, and the circles for heating by substructure and clouds together. The median scaleheight at all luminosities is much larger when heating by clouds is included. However, the scatter in scaleheight at a given luminosity is huge for the case of heating only by substructure, reflecting the strongly stochastic nature of this process. Our calculations predict that brighter galaxies should host thinner disks than fainter galaxies (when measured in terms of fractional disk thickness  $h = z_0/R_d$ ). This trend is apparent in calculations both with and without molecular clouds, and reflects a similar trend in the fractional vertical energy  $E_z/M_{\text{disk}}V_{\text{disk}}^2$ .

### 4.4 Comparison with the Milky Way galaxy

It has been conventional to compare predictions for disk scaleheights with the observed value for the Milky Way galaxy. As a way of testing models against the real universe, this comparison has significant drawbacks, since (i) the global parameters of the Milky Way (such as the disk radial scalelength, total luminosity and bulge-to-disk ratio) are in fact quite difficult to determine observationally in comparison with external galaxies, and (ii) the models predict a *distribution* of scaleheights at a given luminosity, and one cannot constrain a distribution well from only one measured point. Therefore we will make only a brief comparison with the Milky Way here, before comparing with the distribution of scaleheights measured for external galaxies in the next section.

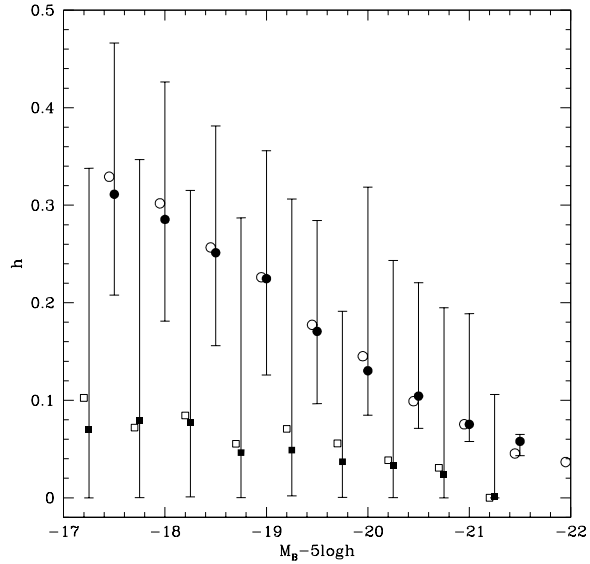


**Figure 7.** The median fractional scale heights  $h = z_0/R_d$  of spiral galaxies as a function of absolute magnitude. The squares show the results for heating by substructure only, and the circles the results for heating by substructure and clouds together. In each case, the filled symbols are for global heating, and the open symbols (offset slightly for clarity) are for local heating. The errorbars indicate the 10% and 90% intervals of the distribution of scaleheights. For clarity, the errorbars are suppressed for the local heating case, but are similar to those for global heating.

The vertical scaleheight of the galactic disk in the solar neighbourhood has been measured from star counts. We use the recent determination by Mendez & Guzman (1998), which for a  $\text{sech}^2(z/z_0)$  vertical profile gives  $z_0 = 0.50 \pm 0.08 \text{kpc}$  (corresponding to an exponential scaleheight of  $0.25 \pm 0.04 \text{kpc}$ ), somewhat smaller than earlier determinations. The measurement of the radial exponential scalelength of the galactic disk has in the past been a matter of more disagreement. We use the models of the galactic mass distribution by Dehnen & Binney (1998), which imply  $R_d = 3.0 \pm 0.4 \text{kpc}$ . Combining these, we find for the fractional scaleheight of the Milky Way stellar disk  $h = z_0/R_d = 0.18 \pm 0.05$ . This range in  $h$  is plotted as a shaded region in Figure 5, from which one can see that the scaleheight of the Milky Way is entirely typical of  $L_*$  disk galaxies in the model (with 35% of galaxies predicted to have  $h > 0.18$ ). We have repeated the comparison using the same definition of ‘Milky Way-like’ galaxies in our model as employed in Benson et al. (2002b), namely a circular velocity at the disk half-mass radius between 210–230km/s and a bulge-to-total ratio by mass between 5–20%. We again find that the observed scaleheight of the Milky Way puts it well within the distribution of  $h$  predicted by the model (with 80% of such galaxies predicted to have  $h > 0.18$ ).

#### 4.5 Comparison with the Observed Scaleheight Distribution for Other Galaxies

The best way to test models of disk heating is to compare their predictions with the observed distribution of scaleheights for external galaxies. This distribution has recently been measured in a complete sample of disk galaxies for the first time by Bizyaev & Mitronova (2002). They measured the vertical and radial scale lengths of a statistically complete sample of 60 edge-on galaxies using the K-band photometry from the 2MASS survey. We compare the scaleheight distribution from their sample with our model predictions in Figure 8. Since the selection criteria for the observational sample are somewhat complex, we weight model galaxies so as to match the distribution of absolute magnitudes found in the observational sample (which peaks in the range  $-19 < M_B - 5 \log h \leq -18$ ), and also select only those galaxies with bulge-to-total luminosity ratios comparable to those of the morphological types found in the observational sample (which are mostly Sc spirals). We see that the model provides quite a good match to the observed distribution, with both distributions peaking around  $h = 0.2$ . The only significant discrepancy is that the model predicts too many systems at large  $h \gtrsim 0.4$ , however it is not clear that such thick galaxies would be recognized observationally as disk galaxies. The conclusions that can be drawn from this comparison are limited by the relatively small size of the observational sample used. However, this situation should soon improve with the availability of data from various large CCD-based sky surveys, allowing much more thorough tests of the theoretical predictions.

## 5 DISCUSSION

We have described a model to calculate the rate of heating of galactic disks by substructures orbiting in their halos. To calibrate this model, we performed several N-body simulations of disk heating and tested these for convergence to ensure accurate results were obtained. We find that the analytical model is able to reproduce the heating rates from N-body simulations to within a factor 2 in most cases. One could perhaps improve the accuracy of the analytical model by treating the satellite-disk interaction in terms of a sum of interactions with resonances in the disk (e.g. Donner & Sundelius 1993; Weinberg & Katz 2002). It is unclear whether such a calculation would ever be worth performing semi-analytically, i.e. whether the computational cost would be any less than a full N-body simulation. Nevertheless, it is clear from the calculations presented in this work that N-body estimates of disk heating rates have their own problems (very large numbers of particles are required in the disk to accurately determine the heating rate), and so it may yet be worthwhile to pursue analytical estimates of disk heating.

We find that for galaxy formation in the standard  $\Lambda$ CDM cosmology, heating by substructure alone produces a distribution of scaleheights which is very broad and skewed to low values, with median fractional scaleheight  $h = z_0/R_d$  around 0.05 for  $L_*$  spiral galaxies. Accounting for additional heating due to stars scattering from gas clouds in the disk

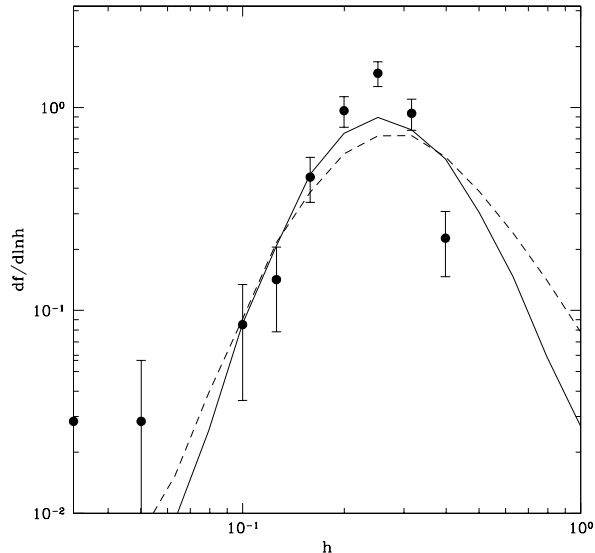


**Figure 8.** The normalized distribution of scale-heights  $h$  from the observational sample of Bizyaev & Mitronova (2002) compared to the prediction from our model. Error bars on the observational datapoints indicate the Poisson errors. The model predictions are shown by solid and dashed lines for global and local heating respectively. The model galaxies have been weighted to match the distribution of absolute magnitudes and morphological types found in the observational sample.

increases the median  $h$  significantly, up to around 0.2. The fractional scaleheight for the Milky Way galaxy, estimated observationally to be around 0.2, is then entirely consistent with what one expects for a typical  $L_*$  spiral galaxy in this model. We find that the predicted distribution of scaleheights for slightly sub- $L_*$  spiral galaxies agrees remarkably well with a recent observational determination by Bizyaev & Mitronova (2002) using data from the 2MASS survey.

There is clearly a need for further study of the heating of galactic disks. In particular the importance of heating by satellite-triggered bars and the extent to which heating is local or global are important, yet poorly understood aspects of this problem. We believe that analytical modeling of the type developed in this paper provides a powerful means to assess the degree of heating by substructure and could easily incorporate any improvements in our understanding of the physics of the process. Its particular strengths are the ability to fully resolve all substructures contributing to the heating and to rapidly compute many realizations of the heating process to allow the full distribution of scaleheights to be determined. These strengths have allowed us to present predicted distributions of galaxy scaleheights which can be tested with forthcoming observational data.

In conclusion, the observed thickness of the Milky Way's stellar disk seems to be entirely consistent with the amount of substructure in galactic halos expected in a cold dark matter universe. The lowest values of  $h$  found for disk galaxies are determined by the heating rate due to star-cloud interactions, while the highest values found are determined by

the heating rate due to substructure. Thus, measurements of the disk scaleheight distribution can potentially constrain these two processes.

## ACKNOWLEDGMENTS

We thank Peter Goldreich, Chung-Pei Ma, Milos Milosavljevic and Simon White for enlightening discussions, James Taylor for providing results from his satellite orbit calculations in electronic form and Volker Springel for making his GADGET N-body code publically available. AJB acknowledges the hospitality of the University of Durham and the Kavli Institute for Theoretical Physics where much of this work was completed. This research was supported in part by the National Science Foundation under Grant No. PHY99-07949.

## REFERENCES

Benson A. J., Cole S., Frenk C. S., Baugh C. M., Lacey C. G., 2000a, MNRAS, 311, 793

Benson A. J., Lacey C. G., Baugh C. M., Cole S., Frenk C. S., 2002a, MNRAS, 333, 156

Benson A. J., Frenk C. S., Lacey C. G., Baugh C. M., Cole S., 2002b, MNRAS, 333, 177

Benson A. J., Lacey C. G., Baugh C. M., Cole S., Frenk C. S., 2002c, submitted to MNRAS (astro-ph/0210354)

Binney J., 1977, MNRAS, 181, 735

Binney J., Tremaine S., 1987, "Galactic Dynamics", Princeton University Press, Princeton

Bizyaev D., Mitronova S., 2002, A&A, 389, 795

Bullock J. S., Kravtsov A. V., Weinberg D. H., 2000, ApJ, 539, 517

Carlberg R. G., Sellwood J. A., 1985, ApJ, 292, 79

Chiba M., 2002, ApJ, 565, 17

Cole S., Lacey C. G., Baugh C. M., Frenk C. S., 2000, MNRAS, 319, 168

Dalal N., Kochanek C. S., 2002a, ApJ, 572, 25

Dalal N., Kochanek C. S., 2002b, submitted to ApJ (astro-ph/0202290)

de Grijp R., Peletier R. F., 1997, A&A, 320, L21

Dehnen W. & Binney J., 1998, MNRAS, 294, 429.

Donner K. J., Sundelius B., 1993, MNRAS, 265, 88

Font A. S., Navarro J. F., Stadel J., Quinn T., 2001, ApJ, 563, L1

Goldreich P., Tremaine S., 1979, ApJ, 233, 857

Granato G. L., Lacey C. G., Silva L., Bressan A., Baugh C. M., Cole S., Frenk C. S., 2000, ApJ, 542, 710

Mendez R. A. & Guzman R., 1998, A&A, 333, 106

Hanninen J. & Flynn C., 2002, MNRAS, 337, 731

Hernquist L., 1993, ApJS, 86, 389

Huang S., Carlberg R. G., 1997, ApJ, 480, 503

King I. R., 1966, AJ, 71, 64

Klypin A. A., Kravtsov A. V., Valenzuela O., Prada F., 1999, ApJ, 522, 82

Lacey C. G., 1984, MNRAS, 208, 687

Lewis J. R., Freeman K. C., 1989, AJ, 97, 139

Metcalfe R. B., Madau P., 2001, ApJ, 563, 9

Moore B., 2001, in J. C. Wheeler and H. Martel eds. "20<sup>th</sup> Texas Symposium on Relativistic Astrophysics", AIP Conference Proceedings, Vol 586, p. 73

Siegel M. H., Majewski S. R., Reid I. N., Thompson I. B., 2002, ApJ, 578, 151

Somerville R. S., 2002, ApJ, 572, 597

Spitzer L., Schwarzschild M., 1953, ApJ, 118, 106

Springel V., Yoshida N., White S. D. M., 2001, NewA, 6, 79

Taffoni G., Mayer L., Colpi M., Governato F., 2003, MNRAS, 341, 434

Taylor J. E., Babul A., 2001, ApJ, 559, 716

Taylor J. E., Babul A., 2003, submitted to MNRAS (astro-ph/0301612)

Tóth G., Ostriker J. P., 1992, ApJ, 389, 5

Velázquez H., White S. D. M., 1999, MNRAS, 304, 254

Villumsen J. V., 1985, ApJ, 290, 75

Wahde M., Donner K. J., Sundelius B., 1996, MNRAS, 281, 1165

Weinberg M. D., Katz N., 2002, ApJ, 580, 627

## APPENDIX A: IMPROVEMENTS IN THE SATELLITE EVOLUTION MODEL

We detail here the changes in the model of satellite evolution compared to Paper I.

i) As before, that mass of a satellite which has become unbound due to tidal forces is lost gradually over a time comparable to the orbital period. The fraction of the unbound mass lost in a small timestep of duration  $\delta t$  was chosen to be proportional to  $\delta t/t_{\text{orb}}$ , where  $t_{\text{orb}}$  is an estimate of the orbital timescale. In Paper I we chose  $t_{\text{orb}} = 2\pi/\omega$ , where  $\omega$  is the instantaneous angular velocity of the satellite. In the present work we instead take  $t_{\text{orb}} = f_{\text{orb}} 2\pi/\sqrt{\omega_{\text{peri}}\omega_{\text{apo}}}$ , where  $\omega_{\text{peri}}$  and  $\omega_{\text{apo}}$  are the angular velocity of the satellite at its most recent pericentric and apocentric passages, and  $f_{\text{orb}}$  is an adjustable parameter which we expect to be of order unity. (Prior to the first pericentric passage we revert to our previous definition of mass loss timescale — this makes little difference to our results as typically very little mass loss occurs prior to this time.) The advantage of this choice is that it produces smoother mass loss histories (as will be shown in §4). Furthermore, when considering cosmological distributions of satellites we occasionally find orbits which become near-radial due to strong dynamical friction forces. The above definition then prevents the mass loss rate from becoming arbitrarily small.

ii) In Chandrasekhar's formula for the dynamical friction force, Taylor & Babul (2001) adopted fixed Coulomb logarithms of  $\ln \Lambda = 2.4$  for the dynamical friction force due to the combined halo/bulge system and  $\ln \Lambda = 0.5$  for the force due to the disk. They found that these values resulted in the best match to the results of the numerical simulations of Velázquez & White (1999; hereafter VW), and we adopted the same values in Paper I. Since we will be interested here in a wide range of satellite and host halo masses, we adopt more general definitions. For the halo and bulge systems we take  $\Lambda_h = f_{\Lambda,h} r (v_{\text{sat}}^2 + \sigma_{1D}^2)/GM_{\text{sat}}$ , where  $r$  is the orbital radius of the satellite,  $M_{\text{sat}}$  its mass,  $v_{\text{sat}}$  the orbital velocity of the satellite,  $\sigma_{1D}$  the one dimensional velocity dispersion of the halo at radius  $r$ , and  $f_{\Lambda,h}$  is a parameter. Since  $\Lambda_h \leq 1$  is possible with this definition, we replace the usual  $\ln \Lambda_h$  term in the expression for the dynamical friction force (eqn. 20 of Paper I) with  $\frac{1}{2} \ln(1 + \Lambda_h^2)$ , the correct form for small  $\Lambda_h$  (Binney & Tremaine 1987). We also account for

the finite size of the satellite as described in Appendix B2. For the disk we must account for the differing scale lengths in radial and vertical directions. A suitable expression for the Coulomb logarithm is derived in Appendix B2.2, and depends on the disk scale length and velocity dispersions, the velocity of the satellite relative to the disk and the angle this velocity makes with the disk plane, and on a parameter  $f_{\Lambda,d}$  which plays a similar role to  $f_{\Lambda,h}$ . These forms are used throughout our calculations.

iii) The disk is now treated as having an anisotropic velocity dispersion ( $\sigma_R, \sigma_\phi, \sigma_z$ ) in the radial, azimuthal and vertical directions, and this anisotropy is included in the calculation of the dynamical friction force due to the disk (see Appendix B2.1). We adopt essentially the same model for the disk velocity dispersion components as VW. For the radial velocity dispersions, we set  $\sigma_R^2 \propto \exp(-R/R_d)$  (Lewis & Freeman 1989)\*\*, where  $R_d$  is the disk radial scale-length, and fix the normalization by assuming the disk to have a Toomre  $Q$ -parameter of 1.5 at its half-mass radius, which results in  $Q \approx 1.5$  at the Solar radius in a Milky Way-like galaxy disk (VW). The azimuthal velocity dispersion is then determined using the epicyclic approximation,  $\sigma_\phi^2 = \sigma_R^2 \kappa^2 / 4\Omega^2$  (where  $\kappa$  is the epicyclic frequency and  $\Omega$  the orbital frequency of the disk). The vertical velocity dispersion at each radius is calculated from the vertical scale-height  $z_0$ , assumed constant with radius, using the expressions in §2.2.2 (the vertical scaleheight in turn is related to the disk vertical energy). In the analytical disk-heating calculation, the radial and azimuthal velocity dispersions are kept fixed in time, but the vertical velocity dispersion evolves with the disk vertical energy.

iv) When computing the dynamical friction force due to the disk, we smooth the disk density to account for the finite size of the satellite halo as did Taylor & Babul (2001). We smooth on a scale equal to the current radius of the satellite after tidal limitation and gravitational shock heating.

v) As the disk scale-height will increase as a function of time due to disk heating, we allow for a variable disk scale height in our satellite orbit calculations. This affects both the dynamical friction force due to the disk and also the gravitational forces exerted by the disk.

vi) Heating by gravitational shocks causes shells of material within a satellite to expand before they become completely unbound. Previously, this effect was included in the calculation of the tidal mass loss, but not in the calculation of the final internal structure. We now calculate the evolution of the internal density and circular velocity profile assuming that the radii of shells of dark matter scale in inverse proportion to their energy. We have repeated the comparison we performed in Paper I of the distribution of peak internal circular velocities of satellite halos predicted by the semi-analytical model with the results of cosmological N-body simulations. We find that the same choice of initial satellite orbital parameters as in Paper I still gives the best match to the N-body simulations.

\*\* Note that VW contains an error in this equation, although the text of that paper is correct.

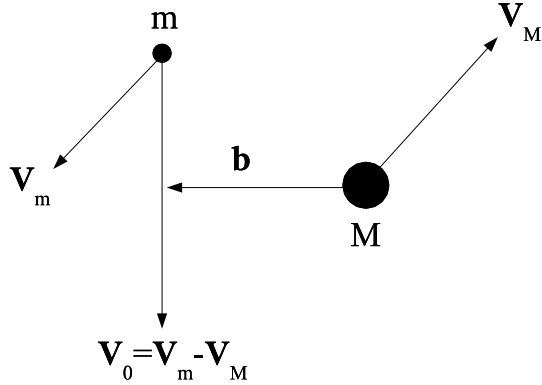


**Figure B1.** The geometry of a scattering event contributing to the dynamical friction force on mass  $M$  due to a particle of mass  $m$ .

## APPENDIX B: DYNAMICAL FRICTION FORMULAE

In this appendix we derive several formulae related to dynamical friction which are employed in this work. For completeness, in §B1 and §B2 we derive several well-known relations relevant to dynamical friction. A more complete discussion of these results can be found in Binney & Tremaine (1987) for example. We consider a mass  $M$  moving through an infinite and homogeneous sea of particles of mass  $m$  ( $\ll M$ ), number density  $n$  and density  $\rho = mn$ .

### B1 Single Scattering Events

For a single scattering event we take the results of Binney & Tremaine (1987; page 422). The scattering geometry is illustrated in Fig. B1. The changes in  $M$ 's velocity parallel and perpendicular to the initial relative velocity vector of the  $m$  and  $M$ ,  $\mathbf{V}_0$ , are:

$$\Delta \mathbf{V}_{||} = \frac{2m}{M} \left[ 1 + \frac{b^2 V_0^4}{G^2 M^2} \right]^{-1} \mathbf{V}_0, \quad (B1)$$

and

$$\Delta \mathbf{V}_{\perp} = \frac{2m V_0^3}{GM^2} \left[ 1 + \frac{b^2 V_0^4}{G^2 M^2} \right]^{-1} \mathbf{b}, \quad (B2)$$

where  $b$  is the impact parameter and we have assumed the background particles to be much less massive than the object for which the force is being calculated.

### B2 Rate of Change of Velocity

We now envisage a sea of particles  $m$  with a distribution of velocities given by  $f(\mathbf{V})$ . The contribution to the rate

of change of velocity in the parallel direction from particles with velocity  $\mathbf{V}$  is simply

$$\frac{d\mathbf{V}_{||}}{dt} = f(\mathbf{V}) \int_0^{b_{\max}} 2\pi b n \mathbf{V}_0 \Delta V_{||} db. \quad (B3)$$

This gives,

$$\frac{dV_{||}}{dt} = 2\pi \ln(1 + \Lambda^2) \rho G^2 M f(\mathbf{V}) \frac{\mathbf{V}_0}{V_0^3}, \quad (B4)$$

where  $\Lambda = b_{\max} V_0^2 / GM$ . If  $M$  has a finite extent (corresponding to replacing the lower integration limit of 0 with  $b_{\min}$ ), the above equation still holds with an effective  $\Lambda$  given by

$$\Lambda_{\text{eff}} = \left( \frac{1 + \Lambda^2}{1 + [b_{\min}/b_{\max}]^2 \Lambda^2} - 1 \right)^{1/2}. \quad (B5)$$

Throughout this work, we take  $b_{\min}$  equal to half the current tidal radius of the satellite.

Clearly, the net change in the velocity of the scatterer perpendicular to  $\mathbf{V}_0$  is zero by symmetry. Thus, the net rate of change of velocity of  $M$  is

$$\frac{d\mathbf{V}_M}{dt} = 2\pi \ln(1 + \Lambda^2) \rho G^2 M \int f(\mathbf{V}) \frac{(\mathbf{V} - \mathbf{V}_{\text{scat}})}{(\mathbf{V} - \mathbf{V}_{\text{scat}})^3} d^3 \mathbf{V}. \quad (B6)$$

The integral in the above equation has an identical form to integrals used to find the gravitational force at position  $x_0$  due to a density distribution, if we identify  $f(\mathbf{V}) \equiv G\rho(\mathbf{x})$ ,  $\mathbf{V} \equiv \mathbf{x}$  and  $\mathbf{V}_{\text{scat}} \equiv \mathbf{x}_0$ .

Thus, the power extracted from the body through dynamical friction is given by,

$$\begin{aligned} P_{\text{scat}} &= M \mathbf{V}_{\text{scat}} \cdot \frac{d\mathbf{V}_{\text{scat}}}{dt} \\ &= 2\pi \ln(1 + \Lambda^2) \rho G^2 M^2 \\ &\quad \mathbf{V}_{\text{scat}} \cdot \int f(\mathbf{V}) \frac{(\mathbf{V} - \mathbf{V}_{\text{scat}})}{(\mathbf{V} - \mathbf{V}_{\text{scat}})^3} d^3 \mathbf{V}. \end{aligned} \quad (B7)$$

### B2.1 Application to an Arbitrary Velocity Ellipsoid

Binney (1977) derives an expression for the dynamical friction force due to a system of particles with uniform density and Gaussian velocity distribution with dispersion  $\sigma_{\perp}$  in one direction and  $\sigma_{||}$  in the other two directions. Binney's equation (A4) is trivially generalized to the case where the velocity dispersions differ in all three directions. Combining this with his equation (A3) we find the following expression for the dynamical friction force:

$$\begin{aligned} \mathbf{F}_{\text{df}} &= \sqrt{2\pi} \ln(1 + \Lambda^2) \rho G^2 M^2 \frac{\sqrt{(1 - e_{\phi}^2)(1 - e_z^2)}}{\sigma_R \sigma_{\phi} \sigma_z} \\ &\quad \times (B_R v_R \hat{\mathbf{e}}_R + B_{\phi} v_{\phi} \hat{\mathbf{e}}_{\phi} + B_z v_z \hat{\mathbf{e}}_z) \end{aligned} \quad (B8)$$

where  $\rho$  is the background density,  $M$  the mass of the orbiting object,  $(v_R, v_{\phi}, v_z)$  is the relative velocity vector of object and background particles (in cylindrical polar coordinates since we will apply this expression to a galaxy disk),  $\hat{\mathbf{e}}_R, \hat{\mathbf{e}}_{\phi}, \hat{\mathbf{e}}_z$  are the basis vectors of the cylindrical polar coordinate system. The coefficients  $B$  are given by,

$$B_R = \int_0^{\infty} \frac{dq}{[(1 + q)^3(1 - e_{\phi}^2 + q)(1 - e_z^2 + q)]^{1/2}}$$

$$\begin{aligned} &\times \exp \left( -\frac{1}{2} \left[ \frac{v_R^2 / \sigma_R^2}{(1 + q)} + \frac{v_{\phi}^2 / \sigma_{\phi}^2}{(1 - e_{\phi}^2 + q)} \right. \right. \\ &\quad \left. \left. + \frac{v_z^2 / \sigma_z^2}{(1 - e_z^2 + q)} \right] \right), \end{aligned} \quad (B9)$$

$$\begin{aligned} B_{\phi} &= \int_0^{\infty} \frac{dq}{[(1 + q)(1 - e_{\phi}^2 + q)^3(1 - e_z^2 + q)]^{1/2}} \\ &\times \exp \left( -\frac{1}{2} \left[ \frac{v_R^2 / \sigma_R^2}{(1 + q)} + \frac{v_{\phi}^2 / \sigma_{\phi}^2}{(1 - e_{\phi}^2 + q)} \right. \right. \\ &\quad \left. \left. + \frac{v_z^2 / \sigma_z^2}{(1 - e_z^2 + q)} \right] \right), \end{aligned} \quad (B10)$$

$$\begin{aligned} B_z &= \int_0^{\infty} \frac{dq}{[(1 + q)(1 - e_{\phi}^2 + q)(1 - e_z^2 + q)^3]^{1/2}} \\ &\times \exp \left( -\frac{1}{2} \left[ \frac{v_R^2 / \sigma_R^2}{(1 + q)} + \frac{v_{\phi}^2 / \sigma_{\phi}^2}{(1 - e_{\phi}^2 + q)} \right. \right. \\ &\quad \left. \left. + \frac{v_z^2 / \sigma_z^2}{(1 - e_z^2 + q)} \right] \right), \end{aligned} \quad (B11)$$

where  $1 - e_{\phi}^2 = \sigma_{\phi}^2 / \sigma_R^2$  and  $1 - e_z^2 = \sigma_z^2 / \sigma_R^2$ .

### B2.2 Effective Coulomb Logarithm for the Disk

In calculating the dynamical friction force due to the disk we require the Coulomb logarithm,  $\frac{1}{2} \ln(1 + \Lambda^2)$ , where  $\Lambda$  is normally defined as  $\Lambda = b_{\max} V_0^2 / GM$ , where  $V_0$  is the typical relative velocity of the satellite and stars in the disk. We adopt  $V_0^2 = V_{\text{rel}}^2 + (\sigma_R^2 + \sigma_{\phi}^2 + \sigma_z^2)/3$ , where  $V_{\text{rel}}$  is the relative velocity of the satellite and the bulk disk motion, and  $\sigma_R$ ,  $\sigma_{\phi}$  and  $\sigma_z$  are the three components of the disk velocity dispersion.

When computing the dynamical friction force we sum the contributions from all particles with impact parameter  $b$  by integrating around an annulus or radius  $b$  normal to the relative velocity vector of the particles and the satellite. We define  $\phi$  as the angle of a point on this annulus measured from a vector in the plane of the annulus which lies parallel to the disk plane. For the disk, the value of  $b_{\max}$ , the upper limit of integration in eqn. (B3) will vary as a function of  $\phi$ . In the direction corresponding to  $\phi = 0$  (and  $\phi = \pi$ ) the satellite will always see the disk to have a characteristic length of  $R_d$  (the exponential scale length). In perpendicular directions ( $\phi = \pi/2$  and  $\phi = 3\pi/2$ ) a more appropriate characteristic length is  $r_{\text{eff}} = R_d (\cos^2 \theta + h^2 \sin^2 \theta)^{1/2}$ , where  $\theta$  is the angle between the satellite-disk relative velocity vector and the  $z$ -axis, and  $h$  the ratio of disk scale height to scale length. Thus, the effective  $\Lambda$  in direction  $\phi$  is

$$\Lambda = \frac{f_{\Lambda, d} R_d h' V_0^2}{GM}, \quad (B12)$$

where  $h' = (\cos^2 \phi + [\cos^2 \theta + h^2 \sin^2 \theta] \sin^2 \phi)^{1/2}$ . If we account for the finite size of the satellite then:

$$(1 + \Lambda^2)_{\text{eff}} = \frac{1 + \Lambda^2}{1 + (b_{\min} \Lambda / R_d h' f_{\Lambda, d})^2}. \quad (B13)$$

The effective Coulomb logarithm is found by averaging over

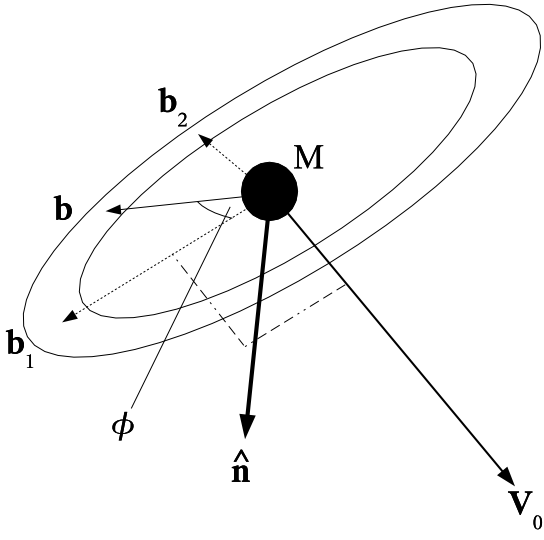


**Figure B2.** Geometry used in computing the rate of increase of velocity dispersion in direction  $\hat{\mathbf{n}}$ . Vectors  $\mathbf{b}$ ,  $\mathbf{b}_1$  and  $\mathbf{b}_2$  lie in the plane of the annulus. Vector  $\mathbf{V}_0$  is normal to the annulus and vector  $\hat{\mathbf{n}}$  lies in the plane of  $\mathbf{V}_0$  and  $\mathbf{b}_1$ .

all  $\phi$ :

$$\left\langle \frac{1}{2} \ln(1 + \Lambda^2)_{\text{eff}} \right\rangle = \frac{1}{4\pi} \int_0^{2\pi} \ln(1 + \Lambda^2)_{\text{eff}} d\phi. \quad (\text{B14})$$

This integral is solved numerically.

### B3 Rate of Increase of Scattered Particle Velocity Dispersion

We now wish to determine the rate of increase of the one-dimensional velocity dispersion, measured in direction  $\hat{\mathbf{n}}$ , of the particles  $m$  due to dynamical friction scatterings. The centre of mass is constant during the scattering,  $m\Delta\mathbf{V}_m + M\Delta\mathbf{V}_M = 0$ . Therefore, to find the change in velocity of  $m$  we multiply the equations (7-10a) and (7-10b) of Binney & Tremaine by  $-M/m$ . Writing these in a more convenient form:

$$\Delta V_{m\perp} = -2V_0 \Lambda \frac{b}{b_{\max}} \left[ 1 + \Lambda^2 \frac{b^2}{b_{\max}^2} \right]^{-1}, \quad (\text{B15})$$

$$\Delta V_{m\parallel} = -2V_0 \left[ 1 + \Lambda^2 \frac{b^2}{b_{\max}^2} \right]^{-1}, \quad (\text{B16})$$

for the components of velocity perpendicular and parallel to the relative velocity vector  $\mathbf{V}_0$  as measured in the frame in which the centre of mass of  $M$  and  $m$  is at rest.

The velocity changes are the same in the frame in which the centre of mass of the central galaxy and its halo is at rest. Hence, the final velocity of  $m$  in that frame is,

$$\mathbf{V}^{(\text{f})} = \mathbf{V} + \frac{\mathbf{V}_0}{V_0} \Delta V_{m\parallel} + \frac{\mathbf{b}}{b} \Delta V_{m\perp}. \quad (\text{B17})$$

We are interested in the velocities in some direction  $\hat{\mathbf{n}}$ . The initial and final velocities of  $m$  in this direction are:

$$\mathbf{V}_{\hat{\mathbf{n}}}^{(\text{i})} = \mathbf{V} \cdot \hat{\mathbf{n}}, \quad (\text{B18})$$

$$\mathbf{V}_{\hat{\mathbf{n}}}^{(\text{f})} = \mathbf{V} \cdot \hat{\mathbf{n}} + \Delta V_{m\parallel} \cos \theta_{V_0} + \Delta V_{m\perp} \cos \theta_b, \quad (\text{B19})$$

where  $\theta_{V_0}$  and  $\theta_b$  are the angles between  $\hat{\mathbf{n}}$  and  $\mathbf{V}_0$  and  $\hat{\mathbf{n}}$  and  $\mathbf{b}$  respectively. The change in the component of the kinetic energy in direction  $\hat{\mathbf{n}}$  is therefore

$$\begin{aligned} \Delta E_{\hat{\mathbf{n}}} = & \frac{m}{2} \{ \Delta V_{m\parallel}^2 \cos^2 \theta_{V_0} + \Delta V_{m\perp}^2 \cos^2 \theta_b \\ & + 2\Delta V_{m\parallel} \Delta V_{m\perp} \cos \theta_{V_0} \cos \theta_b \\ & + 2\mathbf{V} \cdot \hat{\mathbf{n}} [\Delta V_{m\parallel} \cos \theta_{V_0} + \Delta V_{m\perp} \cos \theta_b] \}. \end{aligned} \quad (\text{B20})$$

To sum over all particles  $m$ , we first integrate around an annulus of constant  $|\mathbf{b}|$ . On this annulus,  $\theta_{V_0}$  is constant and we can write the vector  $\mathbf{b} = \mathbf{b}_1 \cos \phi + \mathbf{b}_2 \sin \phi$ , where  $\mathbf{b}_1 \cdot \mathbf{b}_2 = 0$ ,  $|\mathbf{b}_1| = |\mathbf{b}_2| = b$  and  $\phi$  is a parameter (see Fig. B2). We then note that

$$\begin{aligned} \int_0^{2\pi} \cos^2 \theta_b d\phi = & \int_0^{2\pi} \left[ \frac{\mathbf{b}_1 \cdot \hat{\mathbf{n}}}{b} \right]^2 \cos^2 \phi \\ & + \left[ \frac{\mathbf{b}_2 \cdot \hat{\mathbf{n}}}{b} \right]^2 \sin^2 \phi \\ & + 2 \left[ \frac{(\mathbf{b}_1 \cdot \hat{\mathbf{n}})(\mathbf{b}_2 \cdot \hat{\mathbf{n}})}{b^2} \right] \sin \phi \cos \phi d\phi \\ = & \pi \left( \frac{\mathbf{b}_1 \cdot \hat{\mathbf{n}}}{b} \right)^2 + \pi \left( \frac{\mathbf{b}_2 \cdot \hat{\mathbf{n}}}{b} \right)^2. \end{aligned} \quad (\text{B21})$$

If we choose  $\mathbf{b}_1$  to be parallel to the projection of  $\hat{\mathbf{n}}$  into the plane of the annulus then  $\mathbf{b}_1 \cdot \hat{\mathbf{n}}/b = \sin \theta_{V_0}$  and  $\mathbf{b}_2 \cdot \hat{\mathbf{n}}/b = 0$ , so

$$\int_0^{2\pi} \cos^2 \theta_b d\phi = \pi \sin^2 \theta_{V_0}. \quad (\text{B22})$$

Using a similar approach it is simple to show that  $\int_0^{2\pi} \cos \theta_b d\phi = 0$ . Thus, the change in energy becomes

$$\begin{aligned} \Delta E_{\hat{\mathbf{n}}} = & \frac{m}{2} \{ 2\pi \Delta V_{m\parallel}^2 \cos^2 \theta_{V_0} + \pi \Delta V_{m\perp}^2 \sin^2 \theta_{V_0} \\ & + 4\pi \mathbf{V} \cdot \hat{\mathbf{n}} \Delta V_{m\parallel} \cos \theta_{V_0} \}. \end{aligned} \quad (\text{B23})$$

Substituting eqns. (B15) and (B16) we find

$$\begin{aligned} \Delta E_{\hat{\mathbf{n}}} = & \frac{mV_0^2}{2} \left\{ 8\pi \left[ 1 + \Lambda^2 \frac{b^2}{b_{\max}^2} \right]^{-2} \cos^2 \theta_{V_0} \right. \\ & + 4\pi \Lambda^2 \frac{b^2}{b_{\max}^2} \left[ 1 + \Lambda^2 \frac{b^2}{b_{\max}^2} \right]^{-2} \sin^2 \theta_{V_0} \\ & \left. - 8\pi \frac{\mathbf{V} \cdot \hat{\mathbf{n}}}{V_0} \left[ 1 + \Lambda^2 \frac{b^2}{b_{\max}^2} \right]^{-1} \cos \theta_{V_0} \right\}. \end{aligned} \quad (\text{B24})$$

To find the total energy change we multiply by the flux of particles passing through the annulus,  $nV_0 b db$ , and integrate over  $b$  from 0 to  $b_{\max}$ . This gives

$$\begin{aligned} \frac{dE_{\hat{\mathbf{n}}}}{dt} = & \rho V_0^3 b_{\max}^2 \left\{ \frac{2\pi \cos^2 \theta_{V_0}}{1 + \Lambda^2} \right. \\ & \left. + \pi \frac{(1 + \Lambda^2) \ln(1 + \Lambda^2) - \Lambda^2}{\Lambda^2(1 + \Lambda^2)} \sin^2 \theta_{V_0} \right\} \end{aligned}$$

$$-2\pi \frac{\mathbf{V} \cdot \hat{\mathbf{n}}}{V_0} \frac{\ln(1+\Lambda^2)}{\Lambda^2} \cos \theta_{V_0} \Big\}. \quad (\text{B25})$$

We next average over the velocity distribution of  $\mathbf{V}$ . The total rate of energy change is then

$$\frac{dE_{\hat{\mathbf{n}}}}{dt} = \int \rho V_0^3 b_{\max}^2 \left\{ \frac{2\pi \cos^2 \theta_{V_0}}{1+\Lambda^2} \right. \\ \left. + \pi \frac{(1+\Lambda^2) \ln(1+\Lambda^2) - \Lambda^2}{\Lambda^2(1+\Lambda^2)} \sin^2 \theta_{V_0} \right. \\ \left. - 2\pi \frac{\mathbf{V} \cdot \hat{\mathbf{n}}}{V_0} \frac{\ln(1+\Lambda^2)}{\Lambda^2} \cos \theta_{V_0} \right\} f(\mathbf{V}) d^3 \mathbf{V}. \quad (\text{B26})$$

In general it seems that this equation is not analytically solvable, even for  $f(\mathbf{V})$  an isotropic Gaussian. However, if we are interested in systems where random motions are much smaller than the bulk motion (such as galaxy disks) then we can approximate  $f(\mathbf{V}) = \delta(\mathbf{V} - \mathbf{V}_d)$ , where  $\mathbf{V}_d$  is the disk bulk velocity and  $\delta()$  is the Dirac delta function. Note that  $\mathbf{V}_0 = \mathbf{V} - \mathbf{V}_M$  where  $\mathbf{V}_M$  is the velocity of  $M$ . For this case

$$\frac{dE_{\hat{\mathbf{n}}}}{dt} = \rho V_0^3 b_{\max}^2 \left\{ \frac{2\pi \cos^2 \theta_{V_0}}{1+\Lambda^2} \right. \\ \left. + \pi \frac{(1+\Lambda^2) \ln(1+\Lambda^2) - \Lambda^2}{\Lambda^2(1+\Lambda^2)} (1 - \cos^2 \theta_{V_0}) \right. \\ \left. - 2\pi v_d \cos \theta_{v_d} \frac{\ln(1+\Lambda^2)}{\Lambda^2} \cos \theta_{V_0} \right\}, \quad (\text{B27})$$

where  $\cos \theta_{V_0} = v_d \cos \theta_{v_d} - v_M \cos \theta_{v_M}$ . Here  $v_d = V_d/V_0$  and  $\theta_{v_d}$  is the angle between  $\hat{\mathbf{n}}$  and  $\mathbf{V}_d$ , with similar definitions for  $v_M$  and  $\theta_{v_M}$ . The efficiency of energy transfer to direction  $\hat{\mathbf{n}}$  is then easily found by dividing the above by the same expression summed over three orthogonal directions (taking one of these to be parallel to  $\mathbf{V}_0$  simplifies the summation):

$$\epsilon_{\hat{\mathbf{n}}} = \left\{ \frac{2 \cos^2 \theta_{V_0}}{1+\Lambda^2} + \frac{(1+\Lambda^2) \ln(1+\Lambda^2) - \Lambda^2}{\Lambda^2(1+\Lambda^2)} (1 - \cos^2 \theta_{V_0}) \right. \\ \left. - 2v_d \cos \theta_{v_d} \frac{\ln(1+\Lambda^2)}{\Lambda^2} \cos \theta_{V_0} \right\} / \left\{ \frac{2}{1+\Lambda^2} \right. \\ \left. + 2 \frac{(1+\Lambda^2) \ln(1+\Lambda^2) - \Lambda^2}{\Lambda^2(1+\Lambda^2)} \right. \\ \left. - 2v_d \cos \theta_{v_d} \frac{\ln(1+\Lambda^2)}{\Lambda^2} \right\}. \quad (\text{B28})$$

We are interested specifically in the vertical velocity dispersion of a galactic disk. In this case  $\mathbf{V}_d$  lies in the disk plane, while  $\hat{\mathbf{n}}$  is perpendicular to that plane. Consequently  $\cos \theta_{v_d} = 0$  and the above expression simplifies to

$$\epsilon_{\hat{\mathbf{z}}} = \left\{ \frac{2 \cos^2 \theta_{V_0}}{1+\Lambda^2} + \frac{(1+\Lambda^2) \ln(1+\Lambda^2) - \Lambda^2}{\Lambda^2(1+\Lambda^2)} (1 - \cos^2 \theta_{V_0}) \right\} \\ / \left\{ \frac{2}{1+\Lambda^2} + 2 \frac{(1+\Lambda^2) \ln(1+\Lambda^2) - \Lambda^2}{\Lambda^2(1+\Lambda^2)} \right\}. \quad (\text{B29})$$

This expression is then used in eqn. (2) to calculate the vertical heating rate of galaxy disks.

## APPENDIX C: DISK SURFACE ENERGY DENSITIES

We here derive expressions for the different contributions to the surface energy density of the disk. These are used in §2.2.2.

We assume a disk with a density structure

$$\rho_d(R, z) = \Sigma(R) \frac{\operatorname{sech}^2(z/z_0)}{2z_0}. \quad (\text{C1})$$

with  $z_0$  constant with radius. Assuming that the disk is thin,  $z_0 \ll R$ , the potential of the disk can be found by approximating the density distribution as a set of infinite, homogeneous planes, such that

$$\phi_d(R, z) = \int_{-\infty}^{\infty} 2\pi G \rho_d(R, z) |z - z'| dz' + \phi_d(R, 0) \\ = 2\pi G \Sigma(R) z_0 [\ln \cosh(z/z_0) + \ln 2] + \phi_d(R, 0). \quad (\text{C2})$$

Close to the disk plane, the  $z$ -component of the force due to the spherical halo plus bulge is

$$F_h = -\frac{GM_h(R)}{R^3} z, \quad (\text{C3})$$

hence the potential due to these components is

$$\phi_h(R, z) \approx \int_0^z \frac{GM_h(R)}{R^3} z' dz' + \phi_h(R, 0) \\ = \frac{GM_h(R)}{2R^3} z^2 + \phi_h(R, 0). \quad (\text{C4})$$

Referencing all energies to  $z = 0$ , we can neglect the final terms in the above equations. We can now calculate the different contributions to the disk vertical energy per unit area, where necessary using the thin disk approximation  $z_0 \ll R$ . The gravitational self-energy of the disk is then

$$w_{dd}(R) = \frac{1}{2} \int_{-\infty}^{\infty} \phi_d(R, z) \rho_d(R, z) dz \\ = \pi G \Sigma(R)^2 z_0. \quad (\text{C5})$$

The disk-halo gravitational potential energy is

$$w_{dh}(R) = \int_{-\infty}^{\infty} \phi_h(R, z) \rho_d(R, z) dz \\ = \frac{\pi^2 GM_h(R)}{24 R^3} \Sigma_d(R) z_0^2, \quad (\text{C6})$$

and the kinetic energy of the disk is

$$t_z(R) = \frac{1}{2} \Sigma(R) \sigma_z^2(R). \quad (\text{C7})$$

## APPENDIX D: CONVERGENCE TESTS ON N-BODY SIMULATIONS

We repeated the N-body simulations of models G1S1 and G1S5 with double and quadruple the number of particles, labelling these runs G1S1<sup>2</sup>, G1S1<sup>4</sup>, G1S5<sup>2</sup> and G1S5<sup>4</sup>. (In each case we scale the softening in proportion to the mean interparticle separation.) Figures D1 and D2 compare the results for these two models run with different numbers of

particles. We see that the position and velocity of the satellite are well converged up until the very final stages of the satellite's life (at which point it becomes difficult to measure these quantities accurately from the simulation anyway). The higher resolution simulations lose mass from the satellite somewhat more rapidly at late times, but the differences are minor and the mass loss rate is well determined by the simulations. However, the convergence seems poorer for the change in vertical kinetic energy  $\Delta T_z$  (with the energy for the unperturbed disk from model G1S0 subtracted off). For the model G1S5, the difference in the final  $\Delta T_z$  of  $(0.02 - 0.03) \times 10^{14} M_\odot \text{km}^2 \text{s}^{-2}$  between the highest and lowest resolution runs could result mostly from the error in the energy of the unperturbed disk that is subtracted off, since the variation in this value between different realizations is around  $(0.02 - 0.03) \times 10^{14} M_\odot \text{km}^2 \text{s}^{-2}$  in the low resolution case. However, for model G1S1 the differences in  $\Delta T_z$  between the high and low resolution runs are much bigger than can be explained by errors in the subtraction of the unperturbed disk contribution. In this case, the behaviour of  $\Delta T_z$  is not even monotonic as the number of particles is increased. We have investigated this further by repeating some of the lowest resolution simulations using a different sequence of random numbers in generating the initial conditions. We find that this leads to significant variations in  $\Delta T_z$ , comparable to those seen between the lowest resolution and higher resolution simulations. It therefore seems that the amount of disk heating by satellites is sensitive to noise in the initial conditions, over and above the two-body relaxation which heats unperturbed disk. Comparing the highest and lowest resolution runs, we find that the error in the low-resolution estimate of  $\Delta T_z$  is  $\sim 30\%$  for model G1S5, but  $\sim 100\%$  for model G1S1. The convergence of  $\Delta T_z$  with increasing particle number thus seems to depend on the orbital properties of the satellite, with different numbers of particles being required to achieve the same degree of convergence in different cases. A more comprehensive study of convergence in a variety of models will be required to address this question fully.

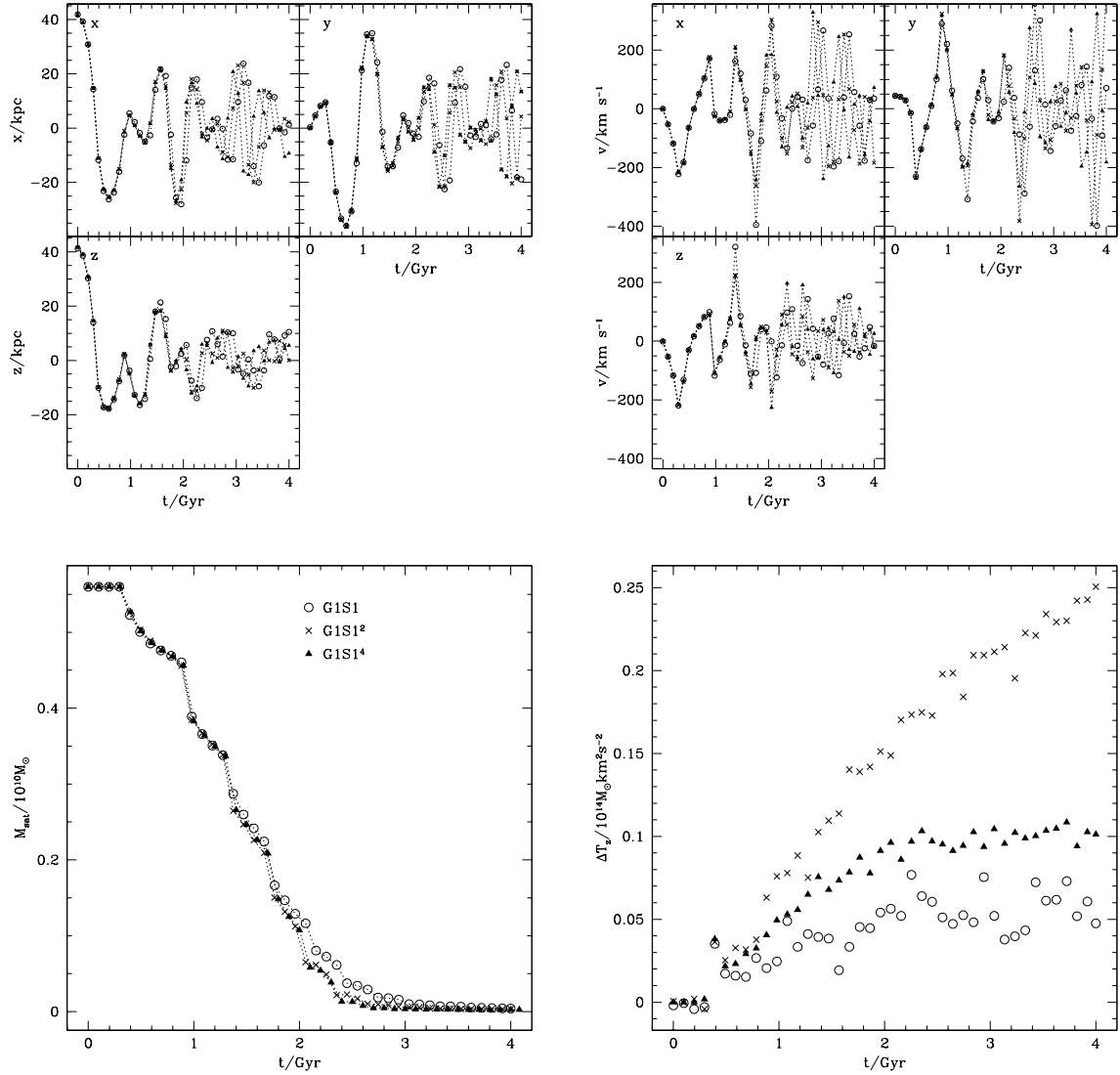


**Figure D1.** Convergence tests for model G1S1. Results are shown for the standard simulation (circles), model G1S1<sup>2</sup> (which has twice the number of particles as G1S1; crosses) and model G1S1<sup>4</sup> (which has four times the number of particles as G1S1; triangles). Points are connected by dotted lines to guide the eye only—lines are not intended as a realistic interpolation of the points. *Top left-hand panel:* The orbital position of the satellite as a function of time. *Top right-hand panel:* The orbital velocity of the satellite as a function of time. *Lower left-hand panel:* The remaining bound mass of the satellite as a function of time. *Lower right-hand panel:* The change in the vertical component of the disk kinetic energy due to heating by the satellite as a function of time.

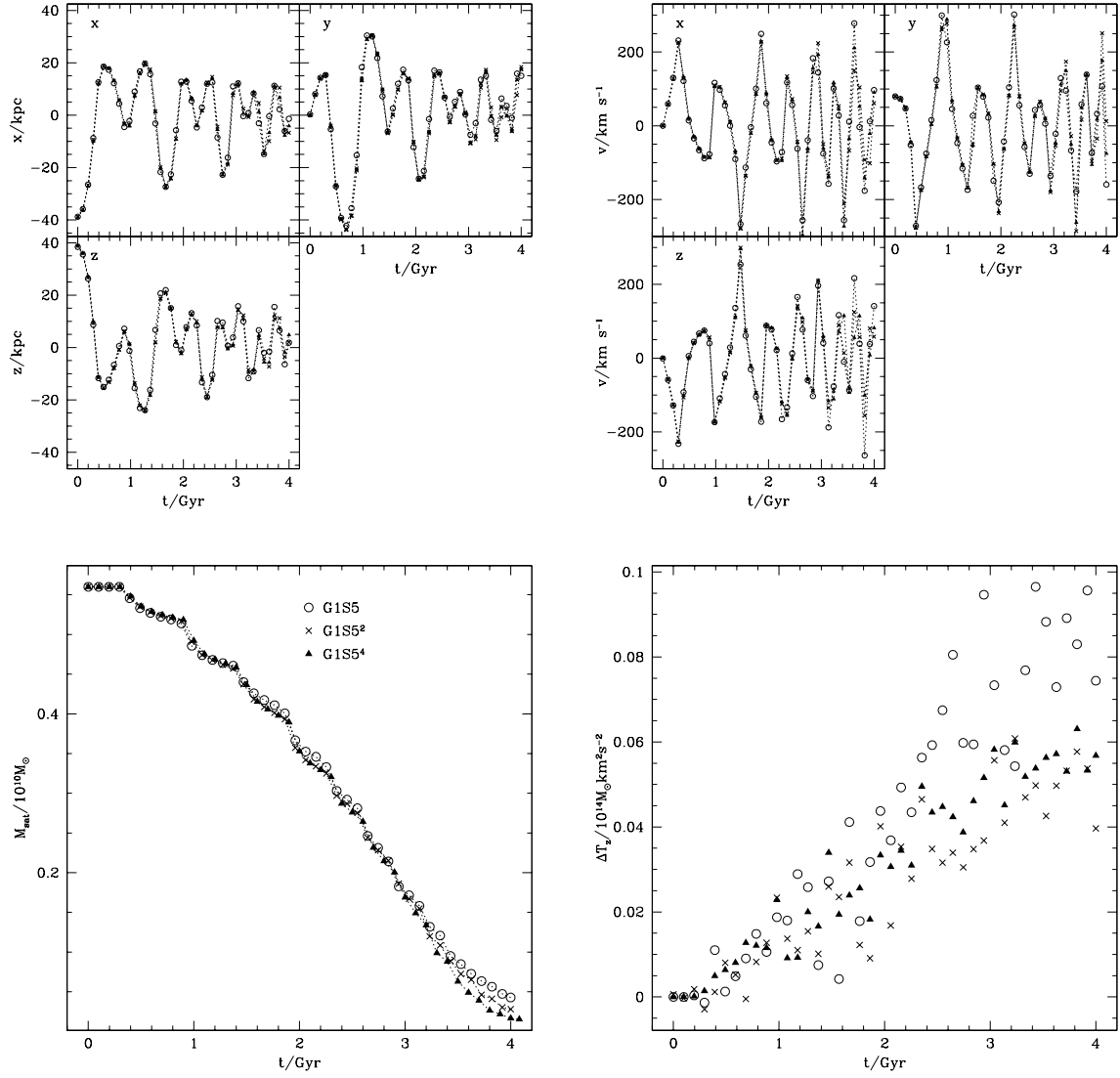


**Figure D2.** Convergence tests for model G1S5. Results are shown for the standard simulation (circles), model G1S5<sup>2</sup> (which has twice the number of particles as G1S5; crosses) and model G1S5<sup>4</sup> (which has four times the number of particles as G1S5; triangles). The different panels are as for Figure D1.